

Amplitude analysis of $D^0 \rightarrow \pi^+ \pi^- \pi^+ \pi^-$ and $D^0 \rightarrow \pi^+ \pi^- \pi^0 \pi^0$ *

M. Ablikim¹, M. N. Achasov^{4,b}, P. Adlarson⁷⁵, O. Afedulidis³, X. C. Ai⁸⁰, R. Aliberti³⁵, A. Amoroso^{74A,74C}, Q. An^{71,58}, Y. Bai⁵⁷, O. Bakina³⁶, I. Balossino^{29A}, Y. Ban^{46,g}, H.-R. Bao⁶³, V. Batozskaya^{1,44}, K. Begzsuren³², N. Berger³⁵, M. Berlowski⁴⁴, M. Bertani^{28A}, D. Bettoni^{29A}, F. Bianchi^{74A,74C}, E. Bianco^{74A,74C}, A. Bortone^{74A,74C}, I. Boyko³⁶, R. A. Briere⁵, A. Brueggemann⁶⁸, H. Cai⁷⁶, X. Cai^{1,58}, A. Calcaterra^{28A}, G. F. Cao^{1,63}, N. Cao^{1,63}, S. A. Cetin^{62A}, J. F. Chang^{1,58}, W. L. Chang^{1,63}, G. R. Che⁴³, G. Chelkov^{36,a}, C. Chen⁴³, C. H. Chen⁹, Chao Chen⁵⁵, G. Chen¹, H. S. Chen^{1,63}, M. L. Chen^{1,58,63}, S. J. Chen⁴², S. L. Chen⁴⁵, S. M. Chen⁶¹, T. Chen^{1,63}, X. R. Chen^{31,63}, X. T. Chen^{1,63}, Y. B. Chen^{1,58}, Y. Q. Chen³⁴, Z. J. Chen^{25,h}, Z. Y. Chen^{1,63}, S. K. Choi^{10A}, X. Chu⁴³, G. Cibinetto^{29A}, F. Cossio^{74C}, J. J. Cui⁵⁰, H. L. Dai^{1,58}, J. P. Dai⁷⁸, A. Dbeyssi¹⁸, R. E. de Boer³, D. Dedovich³⁶, C. Q. Deng⁷², Z. Y. Deng¹, A. Denig³⁵, I. Denysenko³⁶, M. Destefanis^{74A,74C}, F. De Mori^{74A,74C}, B. Ding^{66,1}, X. X. Ding^{46,g}, Y. Ding³⁴, Y. Ding⁴⁰, J. Dong^{1,58}, L. Y. Dong^{1,63}, M. Y. Dong^{1,58,63}, X. Dong⁷⁶, M. C. Du¹, S. X. Du⁸⁰, Z. H. Duan⁴², P. Egorov^{36,a}, Y. H. Fan⁴⁵, J. Fang^{1,58}, J. Fang⁵⁹, S. S. Fang^{1,63}, W. X. Fang¹, Y. Fang¹, Y. Q. Fang^{1,58}, R. Farinelli^{29A}, L. Fava^{74B,74C}, F. Feldbauer³, G. Felici^{28A}, C. Q. Feng^{71,58}, J. H. Feng⁵⁹, Y. T. Feng^{71,58}, K. Fischer⁶⁹, M. Fritsch³, C. D. Fu¹, J. L. Fu⁶³, Y. W. Fu¹, H. Gao⁶³, Y. N. Gao^{46,g}, Yang Gao^{71,58}, S. Garbolino^{74C}, I. Garzia^{29A,29B}, P. T. Ge⁷⁶, Z. W. Ge⁴², C. Geng⁵⁹, E. M. Gersabeck⁶⁷, A. Gilman⁶⁹, K. Goetzen¹³, L. Gong⁴⁰, W. X. Gong^{1,58}, W. Gradl³⁵, S. Gramigna^{29A,29B}, M. Greco^{74A,74C}, M. H. Gu^{1,58}, Y. T. Gu¹⁵, C. Y. Guan^{1,63}, Z. L. Guan²², A. Q. Guo^{31,63}, L. B. Guo⁴¹, M. J. Guo⁵⁰, R. P. Guo⁴⁹, Y. P. Guo^{12,f}, A. Guskov^{36,a}, J. Gutierrez²⁷, K. L. Han⁶³, T. T. Han¹, X. Q. Hao¹⁹, F. A. Harris⁶⁵, K. K. He⁵⁵, K. L. He^{1,63}, F. H. Heinsius³, C. H. Heinz³⁵, Y. K. Heng^{1,58,63}, C. Herold⁶⁰, T. Holtmann³, P. C. Hong^{12,f}, G. Y. Hou^{1,63}, X. T. Hou^{1,63}, Y. R. Hou⁶³, Z. L. Hou¹, B. Y. Hu⁵⁹, H. M. Hu^{1,63}, J. F. Hu^{56,i}, T. Hu^{1,58,63}, Y. Hu¹, G. S. Huang^{71,58}, K. X. Huang⁵⁹, L. Q. Huang^{31,63}, X. T. Huang⁵⁰, Y. P. Huang¹, T. Hussain⁷³, F. Hölzken³, N. Hüsken^{27,35}, N. in der Wiesche⁶⁸, M. Irshad^{71,58}, J. Jackson²⁷, S. Janchiv³², J. H. Jeong^{10A}, Q. Ji¹, Q. P. Ji¹⁹, W. Ji^{1,63}, X. B. Ji^{1,63}, X. L. Ji^{1,58}, Y. Y. Ji⁵⁰, X. Q. Jia⁵⁰, Z. K. Jia^{71,58}, D. Jiang^{1,63}, H. B. Jiang⁷⁶, P. C. Jiang^{46,g}, S. S. Jiang³⁹, T. J. Jiang¹⁶, X. S. Jiang^{1,58,63}, Y. Jiang⁶³, J. B. Jiao⁵⁰, J. K. Jiao³⁴, Z. Jiao²³, S. Jin⁴², Y. Jin⁶⁶, M. Q. Jing^{1,63}, X. M. Jing⁶³, T. Johansson⁷⁵, S. Kabana³³, N. Kalantar-Nayestanaki⁶⁴, X. L. Kang⁹, X. S. Kang⁴⁰, M. Kavatsyuk⁶⁴, B. C. Ke⁸⁰, V. Khachatryan²⁷, A. Khoukaz⁶⁸, R. Kiuchi¹, O. B. Kolcu^{62A}, B. Kopf³, M. Kuessner³, X. Kui^{1,63}, A. Kupsc^{44,75}, W. Kühn³⁷, J. J. Lane⁶⁷, P. Larin¹⁸, L. Lavezzi^{74A,74C}, T. T. Lei^{71,58}, Z. H. Lei^{71,58}, H. Leithoff³⁵, M. Lellmann³⁵, T. Lenz³⁵, C. Li⁴⁷, C. Li⁴³, C. H. Li³⁹, Cheng Li^{71,58}, D. M. Li⁸⁰, F. Li^{1,58}, G. Li¹, H. Li^{71,58}, H. B. Li^{1,63}, H. J. Li¹⁹, H. N. Li^{56,i}, Hui Li⁴³, J. R. Li⁶¹, J. S. Li⁵⁹, Ke Li¹, L. J. Li^{1,63}, L. K. Li¹, Lei Li⁴⁸, M. H. Li⁴³, P. R. Li^{38,k}, Q. M. Li^{1,63}, Q. X. Li⁵⁰, R. Li^{17,31}, S. X. Li¹², T. Li⁵⁰, W. D. Li^{1,63}, W. G. Li¹, X. Li^{1,63}, X. H. Li^{71,58}, X. L. Li⁵⁰, Xiaoyu Li^{1,63}, Y. G. Li^{46,g}, Z. J. Li⁵⁹, Z. X. Li¹⁵, C. Liang⁴², H. Liang^{71,58}, H. Liang^{1,63}, Y. F. Liang⁵⁴, Y. T. Liang^{31,63}, G. R. Liao¹⁴, L. Z. Liao⁵⁰, Y. P. Liao^{1,63}, J. Libby²⁶, A. Limphirat⁶⁰, D. X. Lin^{31,63}, T. Lin¹, B. J. Liu¹, B. X. Liu⁷⁶, C. Liu³⁴, C. X. Liu¹, F. H. Liu⁵³, Fang Liu¹, Feng Liu⁶, G. M. Liu^{56,i}, H. Liu^{38,j,k}, H. B. Liu¹⁵, H. M. Liu^{1,63}, Huanhuan Liu¹, Huihui Liu²¹, J. B. Liu^{71,58}, J. Y. Liu^{1,63}, K. Liu^{38,j,k}, K. Y. Liu⁴⁰, Ke Liu²², L. Liu^{71,58}, L. C. Liu⁴³, Lu Liu⁴³, M. H. Liu^{12,f}, P. L. Liu¹, Q. Liu⁶³, S. B. Liu^{71,58}, T. Liu^{12,f}, W. K. Liu⁴³, W. M. Liu^{71,58}, X. Liu^{38,j,k}, X. Liu³⁹, Y. Liu^{38,j,k}, Y. Liu⁸⁰, Y. B. Liu⁴³, Z. A. Liu^{1,58,63}, Z. D. Liu⁹, Z. Q. Liu⁵⁰, X. C. Lou^{1,58,63}, F. X. Lu⁵⁹, H. J. Lu²³, J. G. Lu^{1,58}, X. L. Lu¹, Y. Lu⁷, Y. P. Lu^{1,58}, Z. H. Lu^{1,63}, C. L. Luo⁴¹, M. X. Luo⁷⁹, T. Luo^{12,f}, X. L. Luo^{1,58}, X. R. Lyu⁶³, Y. F. Lyu⁴³, F. C. Ma⁴⁰, H. Ma⁷⁸, H. L. Ma¹, J. L. Ma^{1,63}, L. L. Ma⁵⁰, M. M. Ma^{1,63}, Q. M. Ma¹, R. Q. Ma^{1,63}, X. T. Ma^{1,63}, X. Y. Ma^{1,58}, Y. Ma^{46,g}, Y. M. Ma³¹, F. E. Maas¹⁸, M. Maggiora^{74A,74C}, S. Malde⁶⁹, A. Mangoni^{28B}, Y. J. Mao^{46,g}, Z. P. Mao¹, S. Marcello^{74A,74C}, Z. X. Meng⁶⁶, J. G. Messchendorp^{13,64}, G. Mezzadri^{29A}, H. Miao^{1,63}, T. J. Min⁴², R. E. Mitchell²⁷, X. H. Mo^{1,58,63}, B. Moses²⁷, N. Yu. Muchnoi^{4,b}, J. Muskalla³⁵, Y. Nefedov³⁶, F. Nerling^{18,d}, I. B. Nikolaev^{4,b}, Z. Ning^{1,58}, S. Nisar^{11,l}, Q. L. Niu^{38,j,k}, W. D. Niu⁵⁵, Y. Niu⁵⁰, S. L. Olsen⁶³, Q. Ouyang^{1,58,63}, S. Pacetti^{28B,28C}, X. Pan⁵⁵, Y. Pan⁵⁷, A. Pathak³⁴, P. Patteri^{28A}, Y. P. Pei^{71,58}, M. Pelizaeus³, H. P. Peng^{71,58}, Y. Y. Peng^{38,j,k}, K. Peters^{13,d}, J. L. Ping⁴¹, R. G. Ping^{1,63}, S. Plura³⁵, V. Prasad³³, F. Z. Qi¹, H. Qi^{71,58},

Received xxxx

* This work is supported in part by National Key R&D Program of China under Contracts Nos. 2020YFA0406300, 2020YFA0406400; National Natural Science Foundation of China (NSFC) under Contracts Nos. 11625523, 11635010, 11735014, 11835012, 11935015, 11935016, 11935018, 11961141012, 12025502, 12035009, 12035013, 12061131003, 12105276, 12122509, 12192260, 12192261, 12192262, 12192263, 12192264, 12192265, 12221005, 12225509, 12235017; the Chinese Academy of Sciences (CAS) Large-Scale Scientific Facility Program; the CAS Center for Excellence in Particle Physics (CCEPP); Joint Large-Scale Scientific Facility Funds of the NSFC and CAS under Contract No. U1732263, U1832103, U1832207, U2032111; CAS Key Research Program of Frontier Sciences under Contracts Nos. QYZDJ-SSW-SLH003, QYZDJ-SSW-SLH040; 100 Talents Program of CAS; The Institute of Nuclear and Particle Physics (INPAC) and Shanghai Key Laboratory for Particle Physics and Cosmology; European Union's Horizon 2020 research and innovation programme under Marie Skłodowska-Curie grant agreement under Contract No. 894790; German Research Foundation DFG under Contracts Nos. 455635585, Collaborative Research Center CRC 1044, FOR5327, GRK 2149; Istituto Nazionale di Fisica Nucleare, Italy; Ministry of Development of Turkey under Contract No. DPT2006K-120470; National Research Foundation of Korea under Contract No. NRF-2022R1A2C1092335; National Science and Technology fund of Mongolia; National Science Research and Innovation Fund (NSRF) via the Program Management Unit for Human Resources & Institutional Development, Research and Innovation of Thailand under Contract No. B16F640076; Polish National Science Centre under Contract No. 2019/35/O/ST2/02907; The Swedish Research Council; U. S. Department of Energy under Contract No. DE-FG02-05ER41374

H. R. Qi⁶¹, M. Qi⁴², T. Y. Qi^{12,f}, S. Qian^{1,58}, W. B. Qian⁶³, C. F. Qiao⁶³, J. J. Qin⁷², L. Q. Qin¹⁴, X. S. Qin⁵⁰, Z. H. Qin^{1,58}, J. F. Qiu¹, S. Q. Qu⁶¹, Z. H. Qu⁷², C. F. Redmer³⁵, K. J. Ren³⁹, A. Rivetti^{74C}, M. Rolo^{74C}, G. Rong^{1,63}, Ch. Rosner¹⁸, S. N. Ruan⁴³, N. Salone⁴⁴, A. Sarantsev^{36,c}, Y. Schelhaas³⁵, K. Schoenning⁷⁵, M. Scodreggio^{29A}, K. Y. Shan^{12,f}, W. Shan²⁴, X. Y. Shan^{71,58}, J. F. Shangguan⁵⁵, L. G. Shao^{1,63}, M. Shao^{71,58}, C. P. Shen^{12,f}, H. F. Shen^{1,8}, W. H. Shen⁶³, X. Y. Shen^{1,63}, B. A. Shi⁶³, H. C. Shi^{71,58}, J. L. Shi¹², J. Y. Shi¹, Q. Q. Shi⁵⁵, R. S. Shi^{1,63}, S. Y. Shi⁷², X. Shi^{1,58}, X. D. Shi^{71,58}, J. J. Song¹⁹, T. Z. Song⁵⁹, W. M. Song^{34,1}, Y. J. Song¹², Y. X. Song^{46,g,m}, S. Sosio^{74A,74C}, S. Spataro^{74A,74C}, F. Stieler³⁵, Y. J. Su⁶³, G. B. Sun⁷⁶, G. X. Sun¹, H. Sun⁶³, H. K. Sun¹, J. F. Sun¹⁹, K. Sun⁶¹, L. Sun⁷⁶, S. S. Sun^{1,63}, T. Sun^{51,e}, W. Y. Sun³⁴, Y. Sun⁹, Y. J. Sun^{71,58}, Y. Z. Sun¹, Z. Q. Sun^{1,63}, Z. T. Sun⁵⁰, C. J. Tang⁵⁴, G. Y. Tang¹, J. Tang⁵⁹, Y. A. Tang⁷⁶, L. Y. Tao⁷², Q. T. Tao^{25,h}, M. Tat⁶⁹, J. X. Teng^{71,58}, V. Thoren⁷⁵, W. H. Tian⁵⁹, Y. Tian^{31,63}, Z. F. Tian⁷⁶, I. Uman^{62B}, Y. Wan⁵⁵, S. J. Wang⁵⁰, B. Wang¹, B. L. Wang⁶³, Bo Wang^{71,58}, D. Y. Wang^{46,g}, F. Wang⁷², H. J. Wang^{38,j,k}, J. P. Wang⁵⁰, K. Wang^{1,58}, L. L. Wang¹, M. Wang⁵⁰, Meng Wang^{1,63}, N. Y. Wang⁶³, S. Wang^{38,j,k}, S. Wang^{12,f}, T. Wang^{12,f}, T. J. Wang⁴³, W. Wang⁵⁹, W. Wang⁷², W. P. Wang^{71,58}, X. Wang^{46,g}, X. F. Wang^{38,j,k}, X. J. Wang³⁹, X. L. Wang^{12,f}, X. N. Wang¹, Y. Wang⁶¹, Y. D. Wang⁴⁵, Y. F. Wang^{1,58,63}, Y. L. Wang¹⁹, Y. N. Wang⁴⁵, Y. Q. Wang¹, Yaqian Wang¹⁷, Yi Wang⁶¹, Z. Wang^{1,58}, Z. L. Wang⁷², Z. Y. Wang^{1,63}, Ziyi Wang⁶³, D. Wei⁷⁰, D. H. Wei¹⁴, F. Weidner⁶⁸, S. P. Wen¹, Y. R. Wen³⁹, U. Wiedner³, G. Wilkinson⁶⁹, M. Wolke⁷⁵, L. Wollenberg³, C. Wu³⁹, J. F. Wu^{1,8}, L. H. Wu¹, L. J. Wu^{1,63}, X. Wu^{12,f}, X. H. Wu³⁴, Y. Wu⁷¹, Y. H. Wu⁵⁵, Y. J. Wu³¹, Z. Wu^{1,58}, L. Xia^{71,58}, X. M. Xian³⁹, B. H. Xiang^{1,63}, T. Xiang^{46,g}, D. Xiao^{38,j,k}, G. Y. Xiao⁴², S. Y. Xiao¹, Y. L. Xiao^{12,f}, Z. J. Xiao⁴¹, C. Xie⁴², X. H. Xie^{46,g}, Y. Xie⁵⁰, Y. G. Xie^{1,58}, Y. H. Xie⁶, Z. P. Xie^{71,58}, T. Y. Xing^{1,63}, C. F. Xu^{1,63}, C. J. Xu⁵⁹, G. F. Xu¹, H. Y. Xu⁶⁶, Q. J. Xu¹⁶, Q. N. Xu³⁰, W. Xu¹, W. L. Xu⁶⁶, X. P. Xu⁵⁵, Y. C. Xu⁷⁷, Z. P. Xu⁴², Z. S. Xu⁶³, F. Yan^{12,f}, L. Yan^{12,f}, W. B. Yan^{71,58}, W. C. Yan⁸⁰, X. Q. Yan¹, H. J. Yang^{51,e}, H. L. Yang³⁴, H. X. Yang¹, Tao Yang¹, Y. Yang^{12,f}, Y. F. Yang⁴³, Y. X. Yang^{1,63}, Yifan Yang^{1,63}, Z. W. Yang^{38,j,k}, Z. P. Yao⁵⁰, M. Ye^{1,58}, M. H. Ye⁸, J. H. Yin¹, Z. Y. You⁵⁹, B. X. Yu^{1,58,63}, C. X. Yu⁴³, G. Yu^{1,63}, J. S. Yu^{25,h}, T. Yu⁷², X. D. Yu^{46,g}, C. Z. Yuan^{1,63}, J. Yuan³⁴, L. Yuan², S. C. Yuan¹, Y. Yuan^{1,63}, Z. Y. Yuan⁵⁹, C. X. Yue³⁹, A. A. Zafar⁷³, F. R. Zeng⁵⁰, S. H. Zeng⁷², X. Zeng^{12,f}, Y. Zeng^{25,h}, Y. J. Zeng⁵⁹, Y. J. Zeng^{1,63}, X. Y. Zhai³⁴, Y. C. Zhai⁵⁰, Y. H. Zhan⁵⁹, A. Q. Zhang^{1,63}, B. L. Zhang^{1,63}, B. X. Zhang¹, D. H. Zhang⁴³, G. Y. Zhang¹⁹, H. Zhang⁷¹, H. C. Zhang^{1,58,63}, H. H. Zhang³⁴, H. H. Zhang⁵⁹, H. Q. Zhang^{1,58,63}, H. Y. Zhang^{1,58}, J. Zhang⁵⁹, J. Zhang⁸⁰, J. J. Zhang⁵², J. L. Zhang²⁰, J. Q. Zhang⁴¹, J. W. Zhang^{1,58,63}, J. X. Zhang^{38,j,k}, J. Y. Zhang¹, J. Z. Zhang^{1,63}, Jianyu Zhang⁶³, L. M. Zhang⁶¹, Lei Zhang⁴², P. Zhang^{1,63}, Q. Y. Zhang^{39,80}, Shuihan Zhang^{1,63}, Shulei Zhang^{25,h}, X. D. Zhang⁴⁵, X. M. Zhang¹, X. Y. Zhang⁵⁰, Y. Zhang⁷², Y. T. Zhang⁸⁰, Y. H. Zhang^{1,58}, Y. M. Zhang³⁹, Yan Zhang^{71,58}, Yao Zhang¹, Z. D. Zhang¹, Z. H. Zhang¹, Z. L. Zhang³⁴, Z. Y. Zhang⁴³, Z. Y. Zhang⁷⁶, G. Zhao¹, J. Y. Zhao^{1,63}, J. Z. Zhao^{1,58}, Lei Zhao^{71,58}, Ling Zhao¹, M. G. Zhao⁴³, R. P. Zhao⁶³, S. J. Zhao⁸⁰, Y. B. Zhao^{1,58}, Y. X. Zhao^{31,63}, Z. G. Zhao^{71,58}, A. Zhemchugov^{36,a}, B. Zheng⁷², J. P. Zheng^{1,58}, W. J. Zheng^{1,63}, Y. H. Zheng⁶³, B. Zhong⁴¹, X. Zhong⁵⁹, H. Zhou⁵⁰, J. Y. Zhou³⁴, L. P. Zhou^{1,63}, X. Zhou⁷⁶, X. K. Zhou⁶, X. R. Zhou^{71,58}, X. Y. Zhou³⁹, Y. Z. Zhou^{12,f}, J. Zhu⁴³, K. Zhu¹, K. J. Zhu^{1,58,63}, L. Zhu³⁴, L. X. Zhu⁶³, S. H. Zhu⁷⁰, S. Q. Zhu⁴², T. J. Zhu^{12,f}, W. J. Zhu^{12,f}, Y. C. Zhu^{71,58}, Z. A. Zhu^{1,63}, J. H. Zou¹, J. Zu^{71,58}

(BESIII Collaboration)

¹ Institute of High Energy Physics, Beijing 100049, People's Republic of China

² Beihang University, Beijing 100191, People's Republic of China

³ Bochum Ruhr-University, D-44780 Bochum, Germany

⁴ Budker Institute of Nuclear Physics SB RAS (BINP), Novosibirsk 630090, Russia

⁵ Carnegie Mellon University, Pittsburgh, Pennsylvania 15213, USA

⁶ Central China Normal University, Wuhan 430079, People's Republic of China

⁷ Central South University, Changsha 410083, People's Republic of China

⁸ China Center of Advanced Science and Technology, Beijing 100190, People's Republic of China

⁹ China University of Geosciences, Wuhan 430074, People's Republic of China

¹⁰ Chung-Ang University, Seoul, 06974, Republic of Korea

¹¹ COMSATS University Islamabad, Lahore Campus, Defence Road, Off Raiwind Road, 54000 Lahore, Pakistan

¹² Fudan University, Shanghai 200433, People's Republic of China

¹³ GSI Helmholtzcentre for Heavy Ion Research GmbH, D-64291 Darmstadt, Germany

¹⁴ Guangxi Normal University, Guilin 541004, People's Republic of China

¹⁵ Guangxi University, Nanning 530004, People's Republic of China

¹⁶ Hangzhou Normal University, Hangzhou 310036, People's Republic of China

¹⁷ Hebei University, Baoding 071002, People's Republic of China

¹⁸ Helmholtz Institute Mainz, Staudinger Weg 18, D-55099 Mainz, Germany

¹⁹ Henan Normal University, Xinxiang 453007, People's Republic of China

²⁰ Henan University, Kaifeng 475004, People's Republic of China

²¹ Henan University of Science and Technology, Luoyang 471003, People's Republic of China

²² Henan University of Technology, Zhengzhou 450001, People's Republic of China

²³ Huangshan College, Huangshan 245000, People's Republic of China

²⁴ Hunan Normal University, Changsha 410081, People's Republic of China

²⁵ Hunan University, Changsha 410082, People's Republic of China

²⁶ Indian Institute of Technology Madras, Chennai 600036, India

²⁷ Indiana University, Bloomington, Indiana 47405, USA

²⁸ INFN Laboratori Nazionali di Frascati, (A)INFN Laboratori Nazionali di Frascati, I-00044, Frascati, Italy; (B)INFN

- Sezione di Perugia, I-06100, Perugia, Italy; (C)University of Perugia, I-06100, Perugia, Italy
- ²⁹ INFN Sezione di Ferrara, (A)INFN Sezione di Ferrara, I-44122, Ferrara, Italy; (B)University of Ferrara, I-44122, Ferrara, Italy
- ³⁰ Inner Mongolia University, Hohhot 010021, People's Republic of China
- ³¹ Institute of Modern Physics, Lanzhou 730000, People's Republic of China
- ³² Institute of Physics and Technology, Peace Avenue 54B, Ulaanbaatar 13330, Mongolia
- ³³ Instituto de Alta Investigación, Universidad de Tarapacá, Casilla 7D, Arica 1000000, Chile
- ³⁴ Jilin University, Changchun 130012, People's Republic of China
- ³⁵ Johannes Gutenberg University of Mainz, Johann-Joachim-Becher-Weg 45, D-55099 Mainz, Germany
- ³⁶ Joint Institute for Nuclear Research, 141980 Dubna, Moscow region, Russia
- ³⁷ Justus-Liebig-Universität Giessen, II. Physikalisches Institut, Heinrich-Buff-Ring 16, D-35392 Giessen, Germany
- ³⁸ Lanzhou University, Lanzhou 730000, People's Republic of China
- ³⁹ Liaoning Normal University, Dalian 116029, People's Republic of China
- ⁴⁰ Liaoning University, Shenyang 110036, People's Republic of China
- ⁴¹ Nanjing Normal University, Nanjing 210023, People's Republic of China
- ⁴² Nanjing University, Nanjing 210093, People's Republic of China
- ⁴³ Nankai University, Tianjin 300071, People's Republic of China
- ⁴⁴ National Centre for Nuclear Research, Warsaw 02-093, Poland
- ⁴⁵ North China Electric Power University, Beijing 102206, People's Republic of China
- ⁴⁶ Peking University, Beijing 100871, People's Republic of China
- ⁴⁷ Qufu Normal University, Qufu 273165, People's Republic of China
- ⁴⁸ Renmin University of China, Beijing 100872, People's Republic of China
- ⁴⁹ Shandong Normal University, Jinan 250014, People's Republic of China
- ⁵⁰ Shandong University, Jinan 250100, People's Republic of China
- ⁵¹ Shanghai Jiao Tong University, Shanghai 200240, People's Republic of China
- ⁵² Shanxi Normal University, Linfen 041004, People's Republic of China
- ⁵³ Shanxi University, Taiyuan 030006, People's Republic of China
- ⁵⁴ Sichuan University, Chengdu 610064, People's Republic of China
- ⁵⁵ Soochow University, Suzhou 215006, People's Republic of China
- ⁵⁶ South China Normal University, Guangzhou 510006, People's Republic of China
- ⁵⁷ Southeast University, Nanjing 211100, People's Republic of China
- ⁵⁸ State Key Laboratory of Particle Detection and Electronics, Beijing 100049, Hefei 230026, People's Republic of China
- ⁵⁹ Sun Yat-Sen University, Guangzhou 510275, People's Republic of China
- ⁶⁰ Suranaree University of Technology, University Avenue 111, Nakhon Ratchasima 30000, Thailand
- ⁶¹ Tsinghua University, Beijing 100084, People's Republic of China
- ⁶² Turkish Accelerator Center Particle Factory Group, (A)Istinye University, 34010, Istanbul, Turkey; (B)Near East University, Nicosia, North Cyprus, 99138, Mersin 10, Turkey
- ⁶³ University of Chinese Academy of Sciences, Beijing 100049, People's Republic of China
- ⁶⁴ University of Groningen, NL-9747 AA Groningen, The Netherlands
- ⁶⁵ University of Hawaii, Honolulu, Hawaii 96822, USA
- ⁶⁶ University of Jinan, Jinan 250022, People's Republic of China
- ⁶⁷ University of Manchester, Oxford Road, Manchester, M13 9PL, United Kingdom
- ⁶⁸ University of Muenster, Wilhelm-Klemm-Strasse 9, 48149 Muenster, Germany
- ⁶⁹ University of Oxford, Keble Road, Oxford OX13RH, United Kingdom
- ⁷⁰ University of Science and Technology Liaoning, Anshan 114051, People's Republic of China
- ⁷¹ University of Science and Technology of China, Hefei 230026, People's Republic of China
- ⁷² University of South China, Hengyang 421001, People's Republic of China
- ⁷³ University of the Punjab, Lahore-54590, Pakistan
- ⁷⁴ University of Turin and INFN, (A)University of Turin, I-10125, Turin, Italy; (B)University of Eastern Piedmont, I-15121, Alessandria, Italy; (C)INFN, I-10125, Turin, Italy
- ⁷⁵ Uppsala University, Box 516, SE-75120 Uppsala, Sweden
- ⁷⁶ Wuhan University, Wuhan 430072, People's Republic of China
- ⁷⁷ Yantai University, Yantai 264005, People's Republic of China
- ⁷⁸ Yunnan University, Kunming 650500, People's Republic of China
- ⁷⁹ Zhejiang University, Hangzhou 310027, People's Republic of China
- ⁸⁰ Zhengzhou University, Zhengzhou 450001, People's Republic of China
- ^a Also at the Moscow Institute of Physics and Technology, Moscow 141700, Russia
- ^b Also at the Novosibirsk State University, Novosibirsk, 630090, Russia
- ^c Also at the NRC "Kurchatov Institute", PNPI, 188300, Gatchina, Russia
- ^d Also at Goethe University Frankfurt, 60323 Frankfurt am Main, Germany
- ^e Also at Key Laboratory for Particle Physics, Astrophysics and Cosmology, Ministry of Education; Shanghai Key Laboratory for Particle Physics and Cosmology; Institute of Nuclear and Particle Physics, Shanghai 200240, People's Republic of China

^f Also at Key Laboratory of Nuclear Physics and Ion-beam Application (MOE) and Institute of Modern Physics, Fudan University, Shanghai 200443, People's Republic of China

^g Also at State Key Laboratory of Nuclear Physics and Technology, Peking University, Beijing 100871, People's Republic of China

^h Also at School of Physics and Electronics, Hunan University, Changsha 410082, China

ⁱ Also at Guangdong Provincial Key Laboratory of Nuclear Science, Institute of Quantum Matter, South China Normal University, Guangzhou 510006, China

^j Also at MOE Frontiers Science Center for Rare Isotopes, Lanzhou University, Lanzhou 730000, People's Republic of China

^k Also at Lanzhou Center for Theoretical Physics, Lanzhou University, Lanzhou 730000, People's Republic of China

^l Also at the Department of Mathematical Sciences, IBA, Karachi 75270, Pakistan

^m Also at Ecole Polytechnique Federale de Lausanne (EPFL), CH-1015 Lausanne, Switzerland

Abstract Using e^+e^- annihilation data corresponding to an integrated luminosity of 2.93 fb^{-1} taken at the center-of-mass energy $\sqrt{s} = 3.773 \text{ GeV}$ with the BESIII detector, a joint amplitude analysis is performed on the decays $D^0 \rightarrow \pi^+\pi^-\pi^+\pi^-$ and $D^0 \rightarrow \pi^+\pi^-\pi^0\pi^0(\text{non-}\eta)$. The fit fractions of individual components are obtained, and large interferences among the dominant components of $D^0 \rightarrow a_1(1260)\pi$, $D^0 \rightarrow \pi(1300)\pi$, $D^0 \rightarrow \rho(770)\rho(770)$ and $D^0 \rightarrow 2(\pi\pi)_S$ are found in both channels. With the obtained amplitude model, the CP -even fractions of $D^0 \rightarrow \pi^+\pi^-\pi^+\pi^-$ and $D^0 \rightarrow \pi^+\pi^-\pi^0\pi^0(\text{non-}\eta)$ are determined to be $(75.2 \pm 1.1_{\text{stat.}} \pm 1.5_{\text{sys.}})\%$ and $(68.9 \pm 1.5_{\text{stat.}} \pm 2.4_{\text{sys.}})\%$, respectively. The branching fractions of $D^0 \rightarrow \pi^+\pi^-\pi^+\pi^-$ and $D^0 \rightarrow \pi^+\pi^-\pi^0\pi^0(\text{non-}\eta)$ are measured to be $(0.688 \pm 0.010_{\text{stat.}} \pm 0.010_{\text{sys.}})\%$ and $(0.951 \pm 0.025_{\text{stat.}} \pm 0.021_{\text{sys.}})\%$, respectively. The amplitude analysis provides an important model for binning strategy in the measurements of the strong phase parameters of $D^0 \rightarrow 4\pi$ when used to determine the CKM angle $\gamma(\phi_3)$ via the $B^- \rightarrow DK^-$ decay.

Key words BESIII, D^0 meson decays, amplitude analysis, CP -even fraction

1 INTRODUCTION

Precision measurements of the elements of the Cabibbo-Kobayashi-Maskawa (CKM) matrix and the test of the unitarity of the CKM triangle [1, 2] are essential goals in the field of flavour physics. One of the three angles of the unitarity triangle, $\gamma(\phi_3) \equiv \arg(-V_{ud}V_{ub}^*/V_{cd}V_{cb}^*)$, can be measured with the tree-level decay $B^\pm \rightarrow DK^\pm$ through the interference between $B^- \rightarrow D^0K^-$ ($b \rightarrow c\bar{u}s$) and $B^- \rightarrow \bar{D}^0K^-$ ($b \rightarrow u\bar{c}s$), which is one of the most important measurements of LHCb and Belle II. Several approaches have been proposed to measure the γ angle via the decay $B^\pm \rightarrow DK^\pm$ [3–5]. Here, the relative magnitude and phase between the D^0 and \bar{D}^0 decays into the same final states, and the D^0 decay parameters (*e.g.* CP -even fraction F_+) are the critical inputs. With more data collected by the LHCb and Belle II experiments in the coming years, the decay parameters of D^0 (\bar{D}^0) will become the dominant source of uncertainty in the γ measurement. Therefore, precision measurements of the D^0 decay parameters are urgently required to improve the precision of the γ measurement.

The decay $D^0 \rightarrow 4\pi$ is regarded as a sensitive mode to extract the γ angle via $B^- \rightarrow DK^-$. Their CP -even fractions (F_+) and relative strong phase parameters in the different phase space (PHSP) bins (c_i/s_i) serve as the direct inputs in the GLW [3] and GGSZ [5] methods, respectively. A reliable decay amplitude model of $D^0 \rightarrow 4\pi$ is critical to precisely extract F_+ and a model-independent c_i/s_i [6], and to search for CP violation in $D^0 \rightarrow 4\pi$ [7]. Moreover, the four-body D^0 hadronic decays provide an excellent platform to study the two-body decays $D^0 \rightarrow VV$ and $D^0 \rightarrow AP$, where V , A , and P denote vector, axial-vector, and pseudo-scalar mesons, re-

spectively. These decays thus enhance the understanding of the decay dynamics of the D^0 meson [8, 9].

Currently, there are only a limited number of experimental studies of $D^0 \rightarrow 4\pi$. The FOCUS experiment performed an amplitude analysis of $D^0 \rightarrow \pi^+\pi^-\pi^+\pi^-$ based on ~ 6000 candidate events with a background fraction of $\sim 10\%$ [10]. An amplitude analysis of $D^0 \rightarrow \pi^+\pi^-\pi^+\pi^-$ was also carried out with the CLEO-c data, which contain ~ 7000 candidate events with a background fraction of $\sim 20\%$ [11]. However, no amplitude analysis of $D^0 \rightarrow \pi^+\pi^-\pi^0\pi^0$ has been performed yet. BESIII has collected 2.93 fb^{-1} of e^+e^- collision data at the center-of-mass energy $\sqrt{s} = 3.773 \text{ GeV}$, where the $D\bar{D}$ is produced by pair without any additional hadrons. This data sample provides an ideal environment for studying D meson decays with the double tag (DT) technique [12, 13]. In this method, a single tag (ST) candidate requires that only one D meson is reconstructed via ST mode. A DT candidate requires that both of D and \bar{D} are reconstructed via signal mode and ST mode, respectively. Based on this data sample and DT method with three ST modes $\bar{D}^0 \rightarrow K^+\pi^-$, $\bar{D}^0 \rightarrow K^+\pi^-\pi^0$ and $\bar{D}^0 \rightarrow K^+\pi^-\pi^+\pi^-$, we report a joint amplitude analysis of $D^0 \rightarrow \pi^+\pi^-\pi^+\pi^-$ and $D^0 \rightarrow \pi^+\pi^-\pi^0\pi^0(\text{non-}\eta)$. Furthermore, we determine the model-dependent CP -even fractions, the absolute branching fractions, and the fractions of individual components. Throughout this paper, the charge-conjugated processes are always implied.

2 BESIII DETECTOR AND MONTE CARLO SIMULATION

The BESIII detector [14] records symmetric e^+e^- collisions provided by the BEPCII storage ring [15] in the

center-of-mass energy range from 2.0 to 4.95 GeV, with a peak luminosity of $1 \times 10^{33} \text{ cm}^{-2}\text{s}^{-1}$ achieved at $\sqrt{s} = 3.77 \text{ GeV}$. BESIII has collected large data samples in this energy region [16]. The cylindrical core of the BESIII detector covers 93% of the full solid angle and consists of a helium-based multilayer drift chamber (MDC), a plastic scintillator time-of-flight system (TOF), and a CsI(Tl) electromagnetic calorimeter (EMC), which are all enclosed in a superconducting solenoidal magnet providing a 1.0 T magnetic field. The solenoid is supported by an octagonal flux-return yoke with resistive plate counter muon identification modules interleaved with steel. The charged-particle momentum resolution at 1 GeV/c is 0.5%, and the dE/dx resolution is 6% for electrons from Bhabha scattering. The EMC measures photon energies with a resolution of 2.5% (5%) at 1 GeV in the barrel (end cap) region. The time resolution in the TOF barrel region is 68 ps, while that in the end cap region is 110 ps.

Simulated data samples produced with a GEANT4-based [17] Monte Carlo (MC) package, which includes the geometric description [18] of the BESIII detector and the detector response, are used to determine detection efficiencies and to estimate backgrounds. The simulation models the beam energy spread and initial state radiation (ISR) in the e^+e^- annihilations with the generator KKMC [19, 20]. The inclusive MC sample including the production of $D\bar{D}$ pairs (including quantum coherence for the neutral D channels), the non- $D\bar{D}$ decays of the $\psi(3770)$, the ISR production of the J/ψ and $\psi(3686)$ states, and the continuum processes incorporated in KKMC are generated to estimate the background and ST efficiencies. All particle decays are modeled with EVTGEN [21, 22] using branching fractions either taken from the Particle Data Group (PDG) [23], when available, or otherwise estimated with LUNDCHARM [24, 25]. Final state radiation from charged final state particles is incorporated using the PHOTOS package [26]. The PHSP signal MC samples of $D^0 \rightarrow \pi^+\pi^-\pi^+\pi^-$ and $D^0 \rightarrow \pi^+\pi^-\pi^0\pi^0$ are generated in PHSP uniformly and are used to calculate the normalization factor of probability density function (PDF) in the amplitude analysis. The signal MC samples of $D^0 \rightarrow \pi^+\pi^-\pi^+\pi^-$ and $D^0 \rightarrow \pi^+\pi^-\pi^0\pi^0$ (non- η) are generated according to the amplitude analysis results and are used to estimate the DT efficiencies.

3 EVENT SELECTION

Charged tracks detected in the MDC are required to be within a polar angle (θ) range of $|\cos\theta| < 0.93$, where θ is defined with respect to the z axis, which is the symmetry axis of the MDC. The distance of closest approach of these charged tracks to the interaction point must be less than 10 cm along the z axis, and less than 1 cm in the transverse plane. Particle identification (PID) for charged tracks combines measurements of the specific ionization energy loss in the MDC (dE/dx) and the flight

time in the TOF to form likelihoods $\mathcal{L}(h)$ ($h = K, \pi$) for each hadron h hypothesis. The charged kaons and pions are identified by comparing the likelihoods for the kaon and pion hypotheses, $\mathcal{L}(K) > \mathcal{L}(\pi)$ and $\mathcal{L}(\pi) > \mathcal{L}(K)$, respectively.

Photon candidates are identified using showers in the EMC. The deposited energy of each shower must be $> 25 \text{ MeV}$ in the barrel region ($|\cos\theta| < 0.80$) and $> 50 \text{ MeV}$ in the end cap region ($0.86 < |\cos\theta| < 0.92$). To exclude showers that originate from charged tracks, the angle subtended by the EMC shower and the position of the closest charged track at the EMC must be $> 10^\circ$ as measured from the interaction point. To suppress electronic noises and reject showers unrelated to the event, the difference between the EMC time and the event start time is required to be within $[0, 700] \text{ ns}$. The π^0 candidates are reconstructed from pairs of photon candidates with invariant mass being in the interval $(0.115, 0.150) \text{ GeV}/c^2$. To improve the momentum resolution, a kinematic fit constraining the two-photon invariant mass to the known π^0 mass [23] is performed, and the four-momenta updated by this kinematic fit are used in the following analysis.

The signal candidates of $D^0 \rightarrow \pi^+\pi^-\pi^+\pi^-$ and $D^0 \rightarrow \pi^+\pi^-\pi^0\pi^0$ are selected with the DT method [12, 13]. First, the ST \bar{D}^0 mesons are reconstructed with the three hadronic decay modes $\bar{D}^0 \rightarrow K^+\pi^-$, $\bar{D}^0 \rightarrow K^+\pi^-\pi^0$, and $\bar{D}^0 \rightarrow K^+\pi^-\pi^+\pi^-$. Two kinematic variables, the energy difference with respect to the beam energy ΔE and the beam energy constrained mass M_{bc} are defined as

$$\Delta E = E_{\bar{D}^0} - E_{\text{beam}}, \quad (1)$$

$$M_{bc} = \sqrt{E_{\text{beam}}^2 - \vec{p}_{\bar{D}^0}^2}, \quad (2)$$

where E_{beam} is the beam energy, and $E_{\bar{D}^0}$ and $\vec{p}_{\bar{D}^0}$ are the energy and momentum of the ST \bar{D}^0 candidate in the e^+e^- center-of-mass frame. For multiple \bar{D}^0 candidates in each ST mode, only the one with the smallest $|\Delta E|$ is kept for further analysis. To reject the backgrounds from cosmic rays and Bhabha events in the ST mode $\bar{D}^0 \rightarrow K^+\pi^-$, the requirements described in Ref. [27] are applied. To reject the peaking background $\bar{D}^0 \rightarrow K^+K_S^0\pi^-$ in the ST mode $\bar{D}^0 \rightarrow K^+\pi^-\pi^+\pi^-$, the events with $|M(\pi^+\pi^-) - 0.4976| < 0.03 \text{ GeV}/c^2$ are vetoed. To further reject combinatorial backgrounds, the \bar{D}^0 candidates are required to have ΔE within a given interval defined in Table 1, about 3 times the resolution for each ST mode. In the sub-sample containing ST candidates, the signal candidates of $D^0 \rightarrow \pi^+\pi^-\pi^+\pi^-$ and $D^0 \rightarrow \pi^+\pi^-\pi^0\pi^0$ are reconstructed with the π^\pm and π^0 candidates which have not been used in the ST side (namely DT thereafter). Similar kinematic variables ΔE and M_{bc} are formed for signal D^0 candidates, and the corresponding ΔE requirements are listed in Table 1. For multiple signal D^0 candidates, only the one giving the smallest $|\Delta E|$ is kept.

To improve the purity of signal candidates in the amplitude analysis, some further selection criteria are ap-

Table 1: The ΔE requirements for different decay modes.

Decay mode	ΔE (GeV)
$\bar{D}^0 \rightarrow K^+\pi^-$	(-0.027, 0.026)
$\bar{D}^0 \rightarrow K^+\pi^-\pi^0$	(-0.057, 0.043)
$\bar{D}^0 \rightarrow K^+\pi^-\pi^+\pi^-$	(-0.020, 0.018)
$D^0 \rightarrow \pi^+\pi^-\pi^+\pi^-$	(-0.032, 0.028)
$D^0 \rightarrow \pi^+\pi^-\pi^0\pi^0$	(-0.066, 0.041)

plied. The studies based on the inclusive MC sample indicate that most backgrounds from the continuum process $e^+e^- \rightarrow q\bar{q}$ include a K_S^0 in the final state. Therefore, common and secondary vertex fits are performed on all $\pi^+\pi^-$ pairs in the event to reconstruct the K_S^0 candidate. The candidate events are rejected if there exists any K_S^0 candidate with $\pi^+\pi^-$ invariant mass within the interval $|M(\pi^+\pi^-) - 0.4976| < 0.03$ GeV/ c^2 with the decay length greater than twice its resolution. The MC studies also show that most backgrounds from $e^+e^- \rightarrow D^+D^-$ contain the decay $D^- \rightarrow K^+\pi^-\pi^-$ due to its large branching fraction and a similar topology as the signal. The candidate events are rejected if there exists any $K^+\pi^-\pi^-$ combinations with $1.863 < M_{bc}(K^+\pi^-\pi^-) < 1.878$ GeV/ c^2 and $|\Delta E(K^+\pi^-\pi^-)| < 0.03$ GeV. There is also the background from the process $e^+e^- \rightarrow D^0\bar{D}^0$. Events with any $\pi^+\pi^-\pi^0$ combinations satisfying $1.859 < M_{bc}(\pi^+\pi^-\pi^0) < 1.873$ GeV/ c^2 and $-0.057 < \Delta E(\pi^+\pi^-\pi^0) < 0.043$ GeV are rejected to eliminate the background of $D^0 \rightarrow \pi^+\pi^-\pi^0$ in the signal process $D^0 \rightarrow \pi^+\pi^-\pi^0\pi^0$. All of the above backgrounds do not form peaks in the M_{bc} distribution of the signal side. There are also some backgrounds which have the same final states as those in the signal mode and produce peaks in the M_{bc} distributions of both the ST and signal sides. To reject the peaking backgrounds $D^0 \rightarrow K_S^0(\rightarrow \pi^+\pi^-)\pi^+\pi^-$ and $D^0 \rightarrow K^-(\rightarrow \pi^+\pi^-\pi^-)\pi^+$ in the signal process $D^0 \rightarrow \pi^+\pi^-\pi^+\pi^-$, events with $|M(\pi^+\pi^-) - 0.4976| < 0.03$ GeV/ c^2 or $M(\pi^+\pi^-\pi^-) < 0.51$ GeV/ c^2 are vetoed. To reject the peaking backgrounds $D^0 \rightarrow K_S^0(\rightarrow \pi^0\pi^0)\pi^+\pi^-$, $D^0 \rightarrow K_S^0(\rightarrow \pi^+\pi^-)\pi^0\pi^0$ and $D^0 \rightarrow K^-(\rightarrow \pi^-\pi^0)\pi^+\pi^0$ in the signal process $D^0 \rightarrow \pi^+\pi^-\pi^0\pi^0$, events with $0.4376 < M(\pi^0\pi^0) < 0.5276$ GeV/ c^2 or $|M(\pi^+\pi^-) - 0.4976| < 0.03$ GeV/ c^2 or $0.4677 < M(\pi^-\pi^0) < 0.5067$ GeV/ c^2 are vetoed. Since the interference between $D^0 \rightarrow \pi^0\eta(\rightarrow \pi^+\pi^-\pi^0)$ and $D^0 \rightarrow \pi^+\pi^-\pi^0\pi^0$ is negligible, events with $M(\pi^+\pi^-\pi^0) < 0.57$ GeV/ c^2 are also vetoed in the signal process $D^0 \rightarrow \pi^+\pi^-\pi^0\pi^0$. Moreover, we reject events if the energy of the photon from π^0 decays is below 50 MeV, as this indicates an incorrect choice of a soft photon.

4 BACKGROUND STUDY AND SIGNAL EXTRACTION

With all the above selection criteria, the two-dimensional (2D) distributions of M_{bc}^{sig} versus M_{bc}^{tag} of

the survived events are shown in the left columns of Figs. 2 and 3, where M_{bc}^{sig} and M_{bc}^{tag} are for the signal and tag sides, respectively. Typically, the signal events are accumulated around the intersection of M_{bc}^{sig} and M_{bc}^{tag} at the D^0 nominal mass. The background, which arises from miscombinations both in the signal and tag sides (namely BKG I thereafter), is located at the diagonal band. There are also the backgrounds from $e^+e^- \rightarrow D^0\bar{D}^0$ but with the wrong reconstruction of the signal side (namely BKG II) or tag side (namely BKG III), distributed as the vertical and horizontal bands, respectively. Detailed MC studies indicate that most of the backgrounds from $e^+e^- \rightarrow D^0\bar{D}^0$ do not form individual peaks in the distribution of M_{bc}^{sig} or M_{bc}^{tag} . However, there are backgrounds from $e^+e^- \rightarrow D^0\bar{D}^0$ with $\bar{D}^0 \rightarrow K^+\pi^-\pi^0$ (namely BKG IV) or $D^0 \rightarrow \pi^+\pi^-\pi^0\pi^0$ (namely BKG V) with the wrong reconstruction of π^0 , which are exactly the signal but with the wrong reconstruction of π^0 and produce a relatively broad peak in the M_{bc}^{tag} or M_{bc}^{sig} distribution, respectively. There are also the backgrounds of $D^0 \rightarrow K_S^0\pi^+\pi^-$, $D^0 \rightarrow K_S^0\pi^0\pi^0$, $D^0 \rightarrow K^-\pi^+\pi^0$ and $D^0 \rightarrow K_S^0\eta'$ (namely BKG VI), which have analogous final states as the signal with the specific decay modes of $K_S^0 \rightarrow \pi^+\pi^-$, $K_S^0 \rightarrow \pi^0\pi^0$, $K^- \rightarrow \pi^-\pi^0$ and $\eta' \rightarrow \gamma\pi^+\pi^-$. These backgrounds are not directly distinguished from the signal in the M_{bc}^{sig} and M_{bc}^{tag} distributions and are estimated by MC simulation. The corresponding yields are summarized in Table 2.

To extract the ST and DT yields, unbinned maximum likelihood fits are performed on the M_{bc}^{tag} distribution of the remaining ST candidates and the 2D distributions of M_{bc}^{sig} versus M_{bc}^{tag} of the remaining DT events in individual tag modes. In the fit to the M_{bc}^{tag} distribution, the signal shape is described by the MC simulated shape of the truth-matched ST events, and the background shape is described by an ARGUS function with the cut-off parameter fixed at 1.8865 GeV/ c^2 [28]. For the $\bar{D}^0 \rightarrow K^+\pi^-\pi^0$ tag mode, an additional peaking background is considered which represents the wrong reconstruction of π^0 as discussed above. This peaking background shape is described by the MC-simulated shape of the truth-matched ST events convolved with a bifurcated Gaussian function with fixed parameters that are obtained from the fit to the corresponding simulated background events. The results of the fits to the M_{bc}^{tag} distributions are shown in Fig. 1.

Table 2: The estimated numbers of peaking background events. The uncertainties include the statistical uncertainties of the estimated background yields and the uncertainties of the quoted branching fractions of different background processes.

Signal mode	$\pi^+\pi^-\pi^+\pi^-$			$\pi^+\pi^-\pi^0\pi^0$		
	Tag mode	$K^+\pi^-$	$K^+\pi^-\pi^0$	$K^+\pi^-$	$K^+\pi^-\pi^0$	$K^+\pi^-\pi^+\pi^-$
$N(K_S^0\pi^+\pi^-)$	24.7 ± 2.3	42.4 ± 4.3	22.9 ± 2.6	12.6 ± 3.1	27.7 ± 6.2	29.2 ± 6.2
$N(K_S^0\pi^0\pi^0)$	-	-	-	1.7 ± 0.4	4.3 ± 0.9	2.4 ± 0.6
$N(K^-\pi^+\pi^0)$	-	-	-	12.6 ± 1.2	23.1 ± 2.2	24.0 ± 1.8
$N(K_S^0\eta')$	-	-	-	3.0 ± 1.2	3.9 ± 1.7	2.8 ± 1.2

In the fit to the 2D distribution of M_{bc}^{sig} (labelled as y_1) versus M_{bc}^{tag} (labelled as y_2), the signal is described by

$$S(y_1, y_2) \otimes G(y_1; \mu_{y_1}, \sigma_{y_1}) \otimes G(y_2; \mu_{y_2}, \sigma_{y_2}),$$

where $S(y_1, y_2)$ is the signal MC shape derived from the truth-matched events, and $G(\mu, \sigma)$ is the Gaussian function describing the resolution difference between data and MC simulation by fixing the parameters $\mu_{y_{1(2)}}$ and $\sigma_{y_{1(2)}}$ to those from the fits on the one-dimensional M_{bc} distributions.

The BKGI is described by

$$T(y_1 - y_2; \mu, \sigma(y_1 + y_2), n) \times A(y_1; m_{y_1}, z'_{y_1}, \rho'_{y_1}) \\ \times A(y_2; m_{y_2}, z'_{y_2}, \rho'_{y_2}),$$

where T is the student's function defined as $T(y; \mu, \sigma, n) = \frac{\Gamma(n/2+0.5)}{\sigma\sqrt{n\pi}\Gamma(n/2)} [1 + \frac{1}{2}(\frac{y-\mu}{\sigma})^2]^{-\frac{n+1}{2}}$, $\sigma(y_1 + y_2) = \sigma_0 + \sigma_1(y_1 + y_2 - m_{y_1} - m_{y_2})$ and A is the ARGUS function defined as $A(y; m, z, \rho) = y(1 - \frac{y^2}{m^2})^\rho e^{z(1 - \frac{y^2}{m^2})}$. In the fit, only the cut-off parameter $m_{y_{1(2)}}$ is fixed to 1.8865 GeV/ c^2 , the other parameters are free to vary.

The BKGII and BKGIII are described by

$$[S(y_{2(1)}) \otimes G(y_{2(1)}; \mu_{y_{2(1)}}, \sigma_{y_{2(1)}})] \\ \times A(y_{1(2)}; m_{y_{1(2)}}, z_{y_{1(2)}}, \rho_{y_{1(2)}}),$$

where A is the ARGUS function as described above, $S(y_{2(1)})$ is the projection of $S(y_1, y_2)$ on $y_{2(1)}$ and G is the same Gaussian function as described above. In the fit, the parameter $m_{y_{1(2)}}$ is fixed to 1.8865 GeV/ c^2 , $\rho_{y_{1(2)}}$ is fixed to the values obtained from the fits to the inclusive MC sample, and $z_{y_{1(2)}}$ is a free parameter.

The BKGIV is described by

$$B_1(y_1, y_2) \otimes G(y_1; \mu_{y_1}, \sigma_{y_1}) \otimes G(y_2; \mu_{y_2}, \sigma_{y_2}),$$

where $B_1(y_1, y_2)$ is the truth-matched signal MC shape convolved with a bifurcated Gaussian function in y_2 and G is the same Gaussian function as described above. In the fit, the parameters of the bifurcated Gaussian function are fixed to the values obtained from the fit to the M_{bc}^{tag} distribution of the corresponding simulated background events.

The BKGV in $D^0 \rightarrow \pi^+\pi^-\pi^0\pi^0$ is described by

$$B_2(y_1, y_2) \otimes G(y_1; \mu_{y_1}, \sigma_{y_1}) \otimes G(y_2; \mu_{y_2}, \sigma_{y_2}),$$

where $B_2(y_1, y_2)$ is the truth-matched signal MC shape convolved with a bifurcated Gaussian function in y_1 and G is the same Gaussian function as described above. In the fit, the parameters of the bifurcated Gaussian function are fixed to the values obtained from the fit to the M_{bc}^{sig} distribution of the corresponding simulated background events.

The BKGVI is described by

$$B_3(y_1, y_2) \otimes G(y_1; \mu_{y_1}, \sigma_{y_1}) \otimes G(y_2; \mu_{y_2}, \sigma_{y_2}),$$

where $B_3(y_1, y_2)$ is the truth-matched MC shape convolved with a bifurcated Gaussian function in y_1 and G are the Gaussian functions. In the fit, the parameters of the bifurcated Gaussian functions are fixed to the value obtained from the fit to the M_{bc}^{sig} distribution of the corresponding simulated background events from the inclusive MC sample, and the yields are fixed to those summarized in Table 2.

The projections of the 2D fits on M_{bc}^{tag} and M_{bc}^{sig} are shown in Figs. 2 and 3, respectively. The obtained ST and DT yields are summarized in Table 3.

5 AMPLITUDE FORMULA

To improve the resolutions of kinematic variables, a one-constraint kinematic fit with the hypothesis of $D^0 \rightarrow 4\pi$ by constraining the 4π invariant mass to the known D^0 mass [23] is performed on the candidate events, and the updated kinematic variables are used in the amplitude analysis. Using the GPUPWA framework [31], a joint amplitude analysis is performed on the candidate events of $D^0 \rightarrow \pi^+\pi^-\pi^+\pi^-$ and $D^0 \rightarrow \pi^+\pi^-\pi^0\pi^0$ (non- η). The general amplitude of the $D^0 \rightarrow f$ decay is given by

$$A_f(p) = \sum_i \Lambda_i U_i(p), \quad (3)$$

where U_i is the amplitude of the i -th intermediate process with a complex coupling factor Λ_i and p is a set of four-momenta of final states. For the \bar{D}^0 decay amplitude, assuming CP conservation, the CP -conjugate PHSP \bar{p} is

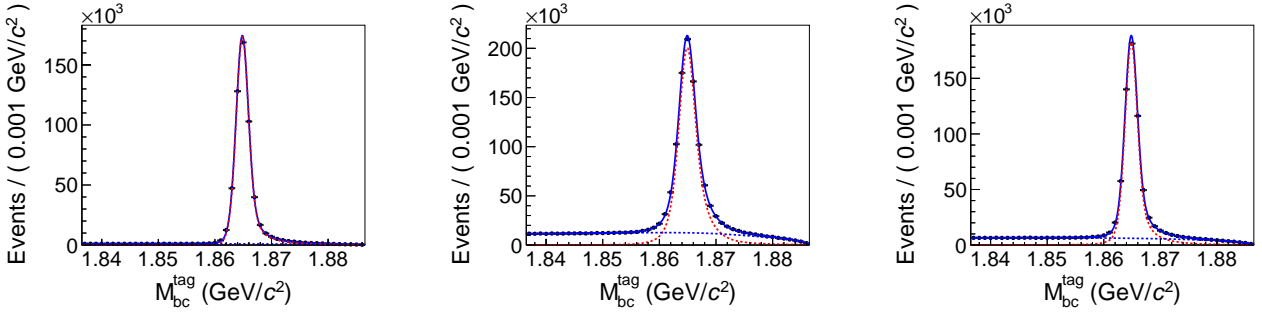


Figure 1: The M_{bc}^{tag} distributions of the ST candidates for $\bar{D}^0 \rightarrow K^+\pi^-$ (left), $\bar{D}^0 \rightarrow K^+\pi^-\pi^0$ (middle) and $\bar{D}^0 \rightarrow K^+\pi^-\pi^+\pi^-$ (right). The dots with error bars are data, the blue solid curves are the total fit results, and the red and blue dashed curves are the signal and background, respectively.

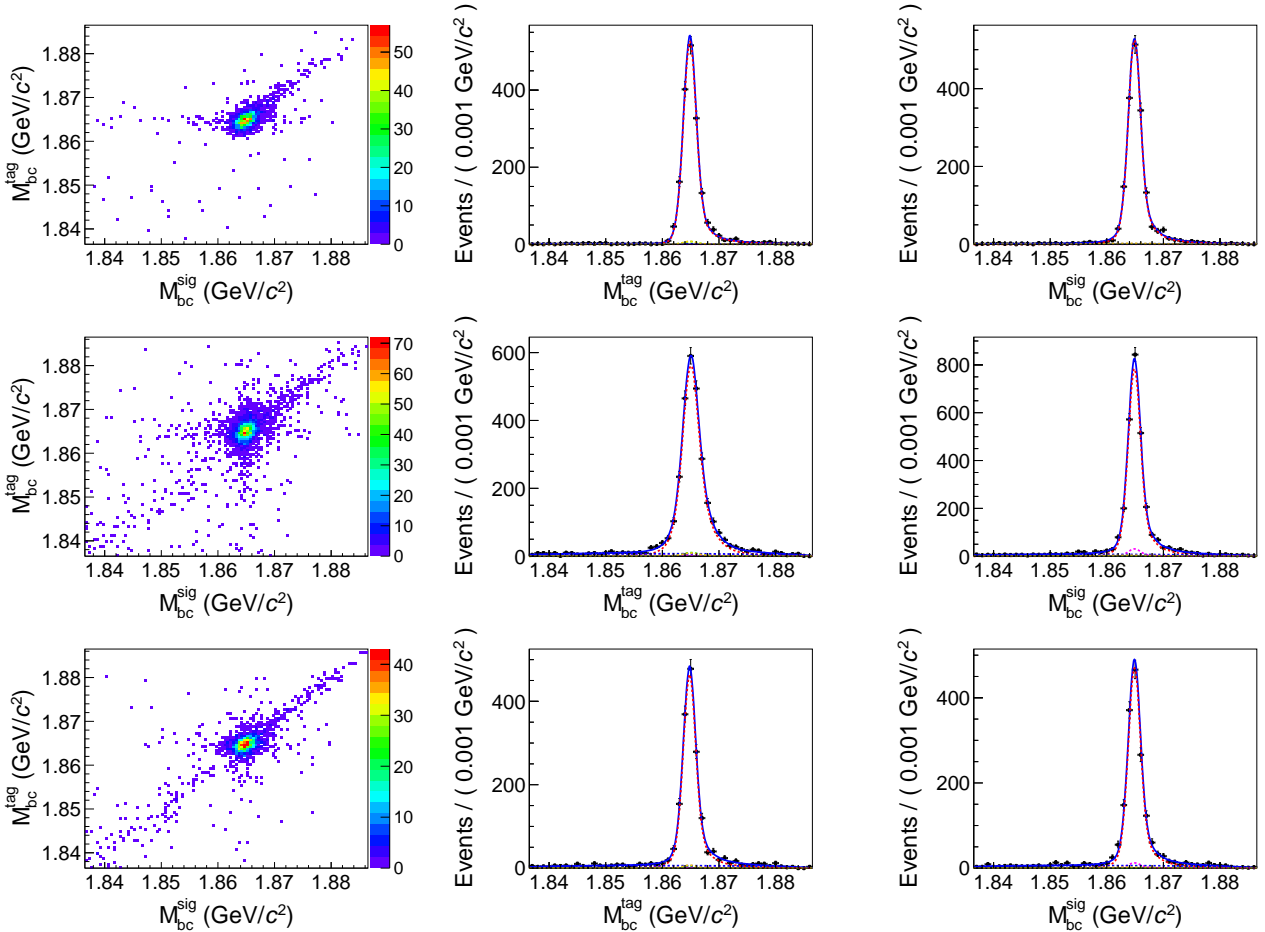


Figure 2: The 2D distributions (left) of M_{bc}^{tag} versus M_{bc}^{sig} and the projections on M_{bc}^{tag} (middle) and M_{bc}^{sig} (right) of the 2D fits on the DT events tagged by $\bar{D}^0 \rightarrow K^+\pi^-$ (first row), $\bar{D}^0 \rightarrow K^+\pi^-\pi^0$ (second row), and $\bar{D}^0 \rightarrow K^+\pi^-\pi^+\pi^-$ (third row) in the $D^0 \rightarrow \pi^+\pi^-\pi^+\pi^-$ decay. The dots with error bars are data. The blue solid curves are the total fit results, and the red dashed curves show the signal. The green, blue, orange, and magenta dashed curves are BKGI, BKIII, BKGVI, and the combination of BKGII and BKGV, respectively.

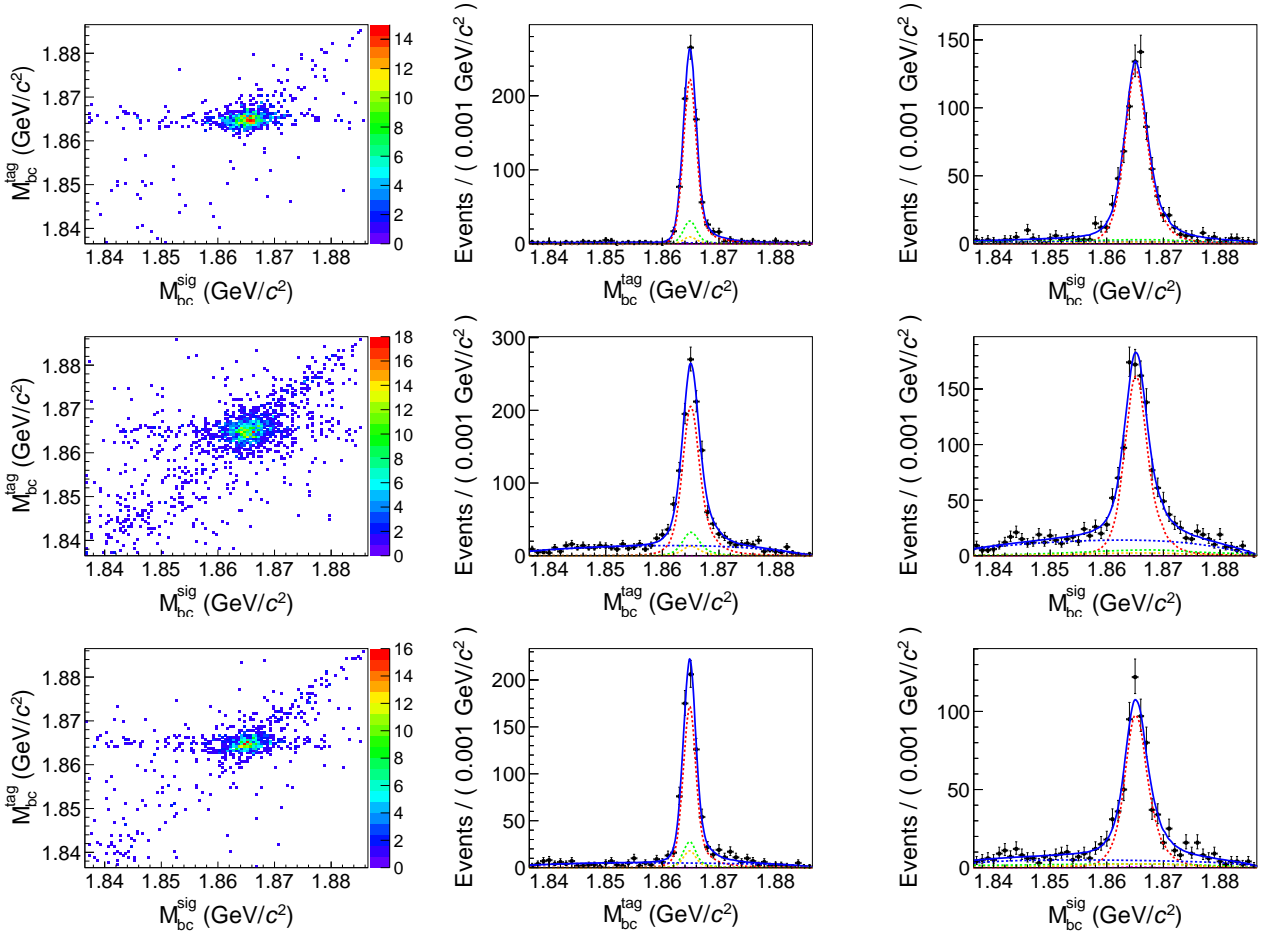


Figure 3: The 2D distributions (left) of M_{bc}^{tag} versus M_{bc}^{sig} and the projections on M_{bc}^{tag} (middle) and M_{bc}^{sig} (right) of the 2D fits on the DT events tagged by $\bar{D}^0 \rightarrow K^+\pi^-$ (first row), $\bar{D}^0 \rightarrow K^+\pi^-\pi^0$ (second row) and $\bar{D}^0 \rightarrow K^+\pi^-\pi^+\pi^-$ (third row) in the $D^0 \rightarrow \pi^+\pi^-\pi^0\pi^0$ decay. The dots with error bars are data. The blue solid curves are the total fit results, and the red dashed curves show the signal. The green dashed curves are the combination of BKG I and BKG IV, the magenta dashed curves are the combination of BKG II and BKG V, the blue and orange dashed curves are BKG III and BKG VI, respectively.

Table 3: The ST and DT yields, efficiencies, and quantum correlated correction factors for three tag modes.

Tag mode	$\bar{D}^0 \rightarrow K^+\pi^-$	$\bar{D}^0 \rightarrow K^+\pi^-\pi^0$	$\bar{D}^0 \rightarrow K^+\pi^-\pi^+\pi^-$
N^{ST}	549586 ± 778	914531 ± 1321	600316 ± 856
ϵ^{ST}	0.6762 ± 0.0004	0.2953 ± 0.0001	0.3365 ± 0.0002
$N_{\pi^+\pi^-\pi^+\pi^-}^{\text{DT}}$	1719 ± 42	2560 ± 56	1520 ± 43
$\epsilon_{\pi^+\pi^-\pi^+\pi^-}^{\text{DT}}$	0.2792 ± 0.0006	0.1187 ± 0.0002	0.1221 ± 0.0003
$N_{\pi^+\pi^-\pi^0\pi^0}^{\text{DT}} \text{ (non-}\eta\text{)}$	721 ± 32	917 ± 39	562 ± 29
$\epsilon_{\pi^+\pi^-\pi^0\pi^0}^{\text{DT}} \text{ (non-}\eta\text{)}$	0.0818 ± 0.0003	0.0319 ± 0.0001	0.0334 ± 0.0001
$\frac{2rR\cos\delta}{1+r^2}$	-0.114 ± 0.004 [29]	-0.067 ± 0.005 [30]	$-0.046^{+0.013}_{-0.011}$ [30]

defined by interchanging the charge of the final state and the reversal of three-momenta. Then, the amplitude of the $\bar{D}^0 \rightarrow \bar{f}$ decay is given as

$$\bar{A}_{\bar{f}}(p) = \sum_i \Lambda_i \bar{U}_i(p) = \sum_i \Lambda_i U_i(\bar{p}) . \quad (4)$$

Since the $D^0\bar{D}^0$ pair is produced in the $\psi(3770)$ decay, quantum correlation between D^0 and \bar{D}^0 needs to be considered. By ignoring the effects of CP violation and $D^0\text{-}\bar{D}^0$ mixing, the observed differential cross section $|M_f(p)|^2$ of $D^0 \rightarrow f$ together with the tag mode $\bar{D}^0 \rightarrow g$ is

$$|A_f(p) - r_g R_g e^{-i\delta_g} \bar{A}_{\bar{f}}(p)|^2 + r_g^2 (1 - R_g^2) |\bar{A}_{\bar{f}}(p)|^2 , \quad (5)$$

where $r_g^2 = \frac{\int |\bar{A}_g|^2 d\Phi_g}{\int |A_g|^2 d\Phi_g}$ and $R_g e^{-i\delta_g} = \frac{\int A_g^* \bar{A}_g d\Phi_g}{\sqrt{\int |A_g|^2 d\Phi_g \int |\bar{A}_g|^2 d\Phi_g}}$. The values of r , R , δ for the three tag modes are summarized in Table 4. In practice, the second term in Eq. (5) is ignored due to the relatively small value of $r_g^2(1 - R_g^2)$.

The amplitude U_i is constructed with the spin factor, Blatt-Weisskopf barrier factors [32], and propagators of resonances. To construct U_i of the four-body D^0 decay, the isobar model is applied in which the decay is factorized into subsequent two-body decay amplitudes [33–35]. The general amplitude of the i -th intermediate process in a four-body decay is given by

$$U_i(p) = S_i(p) B_{L_D}(p) P_{R_1}(p) B_{L_{R_1}}(p) P_{R_2}(p) B_{L_{R_2}}(p) , \quad (6)$$

where S_i is the spin factor of the i -th decay amplitude, B_{L_X} ($X = D, R_1, R_2$) are the Blatt-Weisskopf barrier factors for the D meson and the resonances R_1 and R_2 , and P_{R_1} and P_{R_2} are the propagators of R_1 and R_2 , respectively. The amplitude is constructed with the exchange symmetry for indistinguishable pions.

The spin factor is constructed with the covariant Zemach (Rarita-Schwinger) tensor formalism [36–39] by combining pure-orbital-angular-momentum covariant tensors $\tilde{t}_{\mu_1 \dots \mu_L}^{(L)}$ and the momenta of parent particles together with Minkowski metric $g_{\mu\nu}$ and Levi-Civita symbol $\epsilon_{\mu\nu\lambda\sigma}$. For a process $a \rightarrow bc$, the covariant tensors $\tilde{t}_{\mu_1 \dots \mu_L}^{(L)}$ for the final states of pure orbital angular momentum L are

$$\tilde{t}_{\mu_1 \dots \mu_L}^{(L)} = (-1)^L P_{\mu_1 \dots \mu_L \mu'_1 \dots \mu'_L}^{(L)}(p_a) r^{\mu'_1} \dots r^{\mu'_L} , \quad (7)$$

where $r = p_b - p_c$ and $P_{\mu_1 \dots \mu_L \mu'_1 \dots \mu'_L}^{(L)}(p_a)$ is the spin projection operator of the particle a ,

$$P^{(0)}(p_a) = 1 , \quad (8)$$

$$P_{\mu\mu'}^{(1)}(p_a) = -g_{\mu\mu'} + \frac{p_{a\mu} p_{a\mu'}}{p_a^2} , \quad (9)$$

$$P_{\mu\nu\mu'\nu'}^{(2)}(p_a) = \frac{1}{2} [P_{\mu\mu'}^{(1)}(p_a) P_{\nu\nu'}^{(1)}(p_a) + P_{\mu\nu'}^{(1)}(p_a) P_{\nu\mu'}^{(1)}(p_a)] - \frac{1}{3} P_{\mu\nu}^{(1)}(p_a) P_{\mu'\nu'}^{(1)}(p_a) . \quad (10)$$

Following the isobar model, the spin factors of the four-body decay $D^0 \rightarrow P_1 P_2 P_3 P_4$ are summarized in Table 5.

The Blatt-Weisskopf barrier factors $B_L(q)$ are derived by assuming a square well interaction potential as

$$B_{L=0}(q) = 1 , \quad (11)$$

$$B_{L=1}(q) = \sqrt{\frac{2}{q^2 + q_R^2}} , \quad (12)$$

$$B_{L=2}(q) = \sqrt{\frac{13}{q^4 + 3q^2 q_R^2 + 9q_R^4}} , \quad (13)$$

where q is the momentum of daughter particle in the rest frame of the mother particle, L is the orbital angular momentum, and $q_R - 1/R$ is a hadron ‘‘scale’’ parameter (R denotes the radius of the centrifugal barrier). In this analysis, the radius R is taken to be $5.0 \text{ GeV}^{-1}c$ for D^0 mesons, and $3.0 \text{ GeV}^{-1}c$ for other intermediate resonances.

Generally, the propagators of resonances are described by a relativistic Breit-Wigner function

$$P(s) = \frac{1}{m_0^2 - s - im_0 \Gamma(s)} , \quad (14)$$

where $\Gamma(s)$ is the energy dependent width and m_0 is the nominal mass of the resonance. For a resonance decaying into two scalar particles $a \rightarrow bc$, the energy dependent partial width $\Gamma_{a \rightarrow bc}(s)$ is given by

$$\Gamma_{a \rightarrow bc}(s) = \Gamma_0^{a \rightarrow bc} \left(\frac{q}{q_0} \right)^{2L+1} \left(\frac{m_0}{\sqrt{s}} \right) \left(\frac{B_L(q)}{B_L(q_0)} \right)^2 , \quad (15)$$

where $\Gamma_0^{a \rightarrow bc}$ is the nominal width when $s = m_0^2$ and q_0 is the corresponding momentum of the daughter particle in the rest frame of the mother particle.

In this analysis, the propagators of $\rho(770)$ and $\rho(1450)$ are described by the Gounaris-Sakurai parametrization [40]. The propagator of $f_0(980)$ in the decay $a_1(1420) \rightarrow f_0(980)\pi$ is described by a Flatté parametrization of $\pi\pi$ and KK coupled channels with parameters from Ref. [41].

The K-matrix parametrization [42, 43] instead of the Breit-Wigner formula is adopted for $\pi\pi$ S-wave. The P-vector parametrization of the K-matrix for the $\pi\pi$ S-wave with five coupled channels $\pi\pi$, KK , $\pi\pi\pi\pi$, $\eta\eta$, $\eta\eta'$ and five poles is written as

$$F_\mu(s) = [I - iK(s)\rho(s)]_{\mu\nu}^{-1} P_\nu(s) , \quad (16)$$

where I is the identity matrix, K is the K-matrix describing the scattering process, ρ is the PHSP matrix and P is the initial production vector (P-vector). The indices μ and ν denote the coupled channels ($\pi\pi$, KK , $\pi\pi\pi\pi$, $\eta\eta$, and $\eta\eta'$), and only $F_\mu(s)$ of the $\pi\pi$ component is used as the propagator of the $\pi\pi$ S-wave. The K-matrix is given by

$$K_{\mu\nu}(s) = \left(\sum_\alpha \frac{g_\mu^\alpha g_\nu^\alpha}{m_\alpha^2 - s} + f_{\mu\nu}^{\text{scatt}} \frac{1 - s_0^{\text{scatt}}}{s - s_0^{\text{scatt}}} \right) f_{A0}(s) , \quad (17)$$

which contains five poles ($\alpha = 1$ to 5). The parameters of the K-matrix are fixed to those in Ref. [43]. The P-vector is written as

$$P_\nu(s) = \left(\sum_\alpha \frac{\beta_\alpha g_\nu^\alpha}{m_\alpha^2 - s} + f_\nu^{\text{prod}} \frac{1 - s_0^{\text{prod}}}{s - s_0^{\text{prod}}} \right) , \quad (18)$$

Table 4: The input values of r , R and δ for the three tag modes.

Mode	$K^-\pi^+$	$K^-\pi^+\pi^0$	$K^-\pi^+\pi^-\pi^+$
$r(\%)$	5.86 ± 0.02 [29]	4.41 ± 0.11 [30]	5.50 ± 0.07 [30]
R	1	0.79 ± 0.04 [30]	$0.44^{+0.09}_{-0.10}$ [30]
$\delta(^{\circ})$	$192.1^{+8.6}_{-10.2}$ [29]	196 ± 11 [30]	161^{+28}_{-18} [30]

Table 5: Summary of spin factors in this analysis, where S , P , V , A , T and PT denote scalar, pseudo-scalar, vector, axial-vector, tensor, and pseudo-tensor mesons, respectively. $[S]$, $[P]$, and $[D]$ represent orbital angular momenta $L = 0, 1$, and 2 in the decays, respectively.

Decay chain	Spin factor
$D[S] \rightarrow P P_1, P[S] \rightarrow S P_2, S[S] \rightarrow P_3 P_4$	1
$D[S] \rightarrow P P_1, P[P] \rightarrow V P_2, V[P] \rightarrow P_3 P_4$	$\tilde{t}_\mu(P)\tilde{t}^\mu(V)$
$D[S] \rightarrow P P_1, P[D] \rightarrow T P_2, T[D] \rightarrow P_3 P_4$	$\tilde{t}_{\mu\nu}(P)\tilde{t}^{\mu\nu}(T)$
$D[P] \rightarrow A P_1, A[S] \rightarrow V P_2, V[P] \rightarrow P_3 P_4$	$\tilde{t}_\mu(D)P^{\mu\nu}(A)\tilde{t}_\nu(V)$
$D[P] \rightarrow A P_1, A[D] \rightarrow V P_2, V[P] \rightarrow P_3 P_4$	$\tilde{t}_\mu(D)\tilde{t}^{\mu\nu}(A)\tilde{t}_\nu(V)$
$D[P] \rightarrow A P_1, A[P] \rightarrow S P_2, S[S] \rightarrow P_3 P_4$	$\tilde{t}_\mu(D)\tilde{t}^\mu(A)$
$D[P] \rightarrow A P_1, A[P] \rightarrow T P_2, T[D] \rightarrow P_3 P_4$	$\tilde{t}_\mu(D)\tilde{t}_\nu(A)P^{\mu\nu\rho\sigma}(A)\tilde{t}_{\rho\sigma}(T)$
$D[P] \rightarrow V_1 P_1, V_1[P] \rightarrow V_2 P_2, V_2[P] \rightarrow P_3 P_4$	$\tilde{t}_\mu(D)P^{\mu\nu}(V_1)\epsilon_{\nu\lambda\sigma\alpha}p_{V_1}^\alpha\tilde{t}^\lambda(V_1)\tilde{t}^\sigma(V_2)$
$D[D] \rightarrow PT P_1, PT[S] \rightarrow T P_2, T[D] \rightarrow P_3 P_4$	$\tilde{t}_{\mu\nu}(D)P^{\mu\nu\alpha\beta}(PT)\tilde{t}_{\alpha\beta}(T)$
$D[D] \rightarrow PT P_1, PT[P] \rightarrow V P_2, V[P] \rightarrow P_3 P_4$	$\tilde{t}_{\mu\nu}(D)P^{\mu\nu\alpha\beta}(PT)\tilde{t}_\alpha(PT)\tilde{t}_\beta(V)$
$D[D] \rightarrow PT P_1, PT[D] \rightarrow S P_2, S[S] \rightarrow P_3 P_4$	$\tilde{t}_{\mu\nu}(D)\tilde{t}^{\mu\nu}(PT)$
$D[D] \rightarrow T P_1, T[D] \rightarrow V P_2, V[P] \rightarrow P_3 P_4$	$\tilde{t}_{\mu\nu}(D)P^{\mu\nu\alpha\beta}(T)\epsilon_{\alpha\lambda\sigma\rho}p_T^\rho\tilde{t}_\beta^\lambda(T)P^{\sigma\gamma}(T)\tilde{t}_\gamma(V)$
$D[D] \rightarrow T_1 P_1, T_1[P] \rightarrow T_2 P_2, T_2[D] \rightarrow P_3 P_4$	$\tilde{t}_{\mu\nu}(D)P^{\mu\nu\alpha\beta}(T_1)\epsilon_{\alpha\lambda\sigma\rho}p_{T_1}^\rho\tilde{t}^\lambda(T_1)\tilde{t}_\beta^\sigma(T_2)$
$D[S] \rightarrow S_1 S_2, S_1[S] \rightarrow P_1 P_2, S_2[S] \rightarrow P_3 P_4$	1
$D[P] \rightarrow V S, V[P] \rightarrow P_1 P_2, S[S] \rightarrow P_3 P_4$	$\tilde{t}_\mu(D)\tilde{t}^\mu(V)$
$D[S] \rightarrow V_1 V_2, V_1[P] \rightarrow P_1 P_2, V_2[P] \rightarrow P_3 P_4$	$\tilde{t}_\mu(V_1)\tilde{t}^\mu(V_2)$
$D[P] \rightarrow V_1 V_2, V_1[P] \rightarrow P_1 P_2, V_2[P] \rightarrow P_3 P_4$	$\epsilon_{\mu\nu\alpha\beta}p_D^\beta\tilde{t}^\mu(D)\tilde{t}^\nu(V_1)\tilde{t}^\alpha(V_2)$
$D[D] \rightarrow V_1 V_2, V_1[P] \rightarrow P_1 P_2, V_2[P] \rightarrow P_3 P_4$	$\tilde{t}_{\mu\nu}(D)\tilde{t}^\mu(V_1)\tilde{t}^\nu(V_2)$
$D[D] \rightarrow T S, T[D] \rightarrow P_1 P_2, S[S] \rightarrow P_3 P_4$	$\tilde{t}_{\mu\nu}(D)\tilde{t}^{\mu\nu}(T)$
$D[P] \rightarrow T V, T[D] \rightarrow P_1 P_2, V[P] \rightarrow P_3 P_4$	$\tilde{t}_\mu(D)\tilde{t}^{\mu\nu}(T)\tilde{t}_\nu(V)$
$D[D] \rightarrow T V, T[D] \rightarrow P_1 P_2, V[P] \rightarrow P_3 P_4$	$\epsilon_{\mu\nu\alpha\beta}p_D^\beta\tilde{t}^{\mu\rho}(D)\tilde{t}_\rho^\nu(T)\tilde{t}^\alpha(V)$
$D[S] \rightarrow T_1 T_2, T_1[D] \rightarrow P_1 P_2, T_2[D] \rightarrow P_3 P_4$	$\tilde{t}_{\mu\nu}(T_1)\tilde{t}^{\mu\nu}(T_2)$
$D[P] \rightarrow T_1 T_2, T_1[D] \rightarrow P_1 P_2, T_2[D] \rightarrow P_3 P_4$	$\epsilon_{\mu\nu\alpha\beta}p_D^\beta\tilde{t}^\mu(D)\tilde{t}^{\nu\rho}(T_1)\tilde{t}_\rho^\alpha(T_2)$
$D[D] \rightarrow T_1 T_2, T_1[D] \rightarrow P_1 P_2, T_2[D] \rightarrow P_3 P_4$	$\tilde{t}_{\mu\nu}(D)\tilde{t}^{\mu\rho}(T_1)\tilde{t}_\rho^\nu(T_2)$

where the poles are the same as for the K-matrix. The parameters β_α , $f_{1\nu}^{\text{prod}}$, and s_0^{prod} are free in the fit.

In practice, there are two $\pi\pi$ S-waves in the decay $D^0 \rightarrow S_1 S_2$, and the corresponding propagator is

$$F'_{\mu\nu}(s_1, s_2) = [I - iK(s_1)\rho(s_1)]_{\mu\rho}^{-1} [I - iK(s_2)\rho(s_2)]_{\nu\sigma}^{-1} \times P_{\rho\sigma}(s_1, s_2), \quad (19)$$

where s_1 and s_2 are the invariant masses squared of $\pi\pi$, $P_{\rho\sigma}(s_1, s_2)$ is the expansion of the product of two P-vectors $P_\rho(s_1)$ and $P_\sigma(s_2)$, and the corresponding coefficients of each term are taken to be independent parameters in the fit. Benefiting from the exchange symmetry of two $\pi\pi$ S-waves in the amplitude, $P_{\rho\sigma}(s_1, s_2)$ can be written as

$$P_{\rho\sigma}(s_1, s_2) = \sum_{\alpha, \beta}^{\alpha \leq \beta} a_{\alpha, \beta} \left[\frac{g_\rho^\alpha g_\sigma^\beta}{(m_\alpha^2 - s_1)(m_\beta^2 - s_2)} + \frac{g_\rho^\beta g_\sigma^\alpha}{(m_\beta^2 - s_1)(m_\alpha^2 - s_2)} \right] + \sum_\alpha b_{\alpha, \rho} \frac{g_\sigma^\alpha (1 - s_0^{\text{prod}})}{(s_1 - s_0^{\text{prod}})(m_\alpha^2 - s_2)} + \sum_\alpha b_{\alpha, \sigma} \frac{g_\rho^\alpha (1 - s_0^{\text{prod}})}{(s_2 - s_0^{\text{prod}})(m_\alpha^2 - s_1)} + c_{[\rho, \sigma]} \frac{(1 - s_0^{\text{prod}})^2}{(s_1 - s_0^{\text{prod}})(s_2 - s_0^{\text{prod}})}, \quad (20)$$

where $c_{[\rho, \sigma]} = c_{\rho, \sigma} + c_{\sigma, \rho}$, and $c_{[\rho, \sigma]}$ with $\rho > \sigma$ is fixed to zero in the fit. Similar to one $\pi\pi$ S-wave, only $(\pi\pi, \pi\pi)$ component of $F'_{\mu\nu}$ is used.

The propagators of the resonances $a_1(1260)$, $a_1(1640)$, $h_1(1170)$ and $\pi(1300)$ decaying into 3π are described by relativistic Breit-Wigner functions with energy dependent widths with the coupled channel 3π , where the

$$A(D^0 \rightarrow a_1^+ \pi^-) = A(\rho_{\pi^+ \pi^-}^0 \pi^+, \pi^-) + A(\rho_{\pi^+ \pi^0}^+ \pi^0, \pi^-) - c[2A(f_{\pi^+ \pi^-} \pi^+, \pi^-) + A(f_{\pi^0 \pi^0} \pi^+, \pi^-)], \quad (23)$$

$$A(D^0 \rightarrow a_1^0 \pi^0) = -A(\rho_{\pi^+ \pi^0}^+ \pi^-, \pi^0) + A(\rho_{\pi^0 \pi^-}^- \pi^+, \pi^0) - c[2A(f_{\pi^+ \pi^-} \pi^0, \pi^0) + A(f_{\pi^0 \pi^0} \pi^0, \pi^0)], \quad (24)$$

$$A(D^0 \rightarrow a_1^- \pi^+) = -A(\rho_{\pi^+ \pi^-}^0 \pi^-, \pi^+) - A(\rho_{\pi^0 \pi^-}^- \pi^0, \pi^+) - c[2A(f_{\pi^+ \pi^-} \pi^-, \pi^+) + A(f_{\pi^0 \pi^0} \pi^-, \pi^+)], \quad (25)$$

$$A(D^0 \rightarrow h_1^0 \pi^0) = -A(\rho_{\pi^+ \pi^0}^+ \pi^-, \pi^0) - A(\rho_{\pi^0 \pi^-}^- \pi^+, \pi^0) + A(\rho_{\pi^+ \pi^-}^0 \pi^0, \pi^0), \quad (26)$$

$$A(D^0 \rightarrow f f') = 4A(f_{\pi^+ \pi^-}, f'_{\pi^+ \pi^-}) + 2[A(f_{\pi^+ \pi^-}, f'_{\pi^0 \pi^0}) + A(f_{\pi^0 \pi^0}, f'_{\pi^+ \pi^-})] + A(f_{\pi^0 \pi^0}, f'_{\pi^0 \pi^0}), \quad (27)$$

$$A(D^0 \rightarrow \rho^0 f) = 2A(\rho_{\pi^+ \pi^-}^0, f_{\pi^+ \pi^-}) + A(\rho_{\pi^+ \pi^-}^0, f_{\pi^0 \pi^0}). \quad (28)$$

Here, a_1 and ρ are isospin vectors, whereas h_1 and $f^{(\prime)}$ are isospin scalars. The normalization factors are dropped here and c is the relative difference (including magnitude and phase) between two isospin processes which is determined in the amplitude analysis.

6 AMPLITUDE FIT PROCESS AND RESULT

In the amplitude fit, the sPlot technique [46] is applied to deal with the effect of background. In the sPlot method, the four-momenta of final states are chosen as control variables x , M_{bc}^{sig} and M_{bc}^{tag} are chosen as discrim-

inating variables y , and the weight for each candidate event is obtained by an unbinned maximum likelihood fit on the 2D distribution of M_{bc}^{sig} versus M_{bc}^{tag} , as described in Sec. 4.

$$\Gamma_{a \rightarrow bcd}(s) \propto \frac{1}{m_0} \int \sum_{\text{spin}} |A_{a \rightarrow bcd}|^2 d\Phi_3, \quad (21)$$

based on the amplitudes $A_{R \rightarrow 3\pi}$ obtained in this analysis. For other resonances decaying into 3π , a relativistic Breit-Wigner function with a constant width is used. The parameters of $a_1(1260)$ and $\pi(1300)$ are determined in the fit and others are fixed to their respective PDG values. [23] Due to its small contribution, the $a_1(1420)$ is described as a relativistic Breit-Wigner function with a constant width, even though it has been regarded as the effect of the Triangle Singularity [44]. Only the decay of $a_1(1420) \rightarrow f_0(980)\pi$ is taken into account, and the corresponding resonant parameters are taken from Ref. [45].

To take into account the resolution effect for the narrow resonances $\phi(1020)$ and $\omega(782)$, the shapes of corresponding relativistic Breit-Wigner functions in the $M(\pi^+\pi^-\pi^0)$ distribution are convolved with a Gaussian function. The parameters of this Gaussian function are obtained by the fit to the η peak in the $M(\pi^+\pi^-\pi^0)$ distribution with the Breit-Wigner function of η convolved with the same Gaussian function.

In this analysis, two decay topologies, $D \rightarrow R_1 R_2$ and $D \rightarrow R_1 \pi \rightarrow R_2 \pi \pi$, are considered. Meanwhile, isospin symmetry is considered by applying the Clebsch-Gordan (CG) coefficients between the isospin processes. The isospin states for u and d quarks are

$$|u\rangle : \left| \frac{1}{2}, \frac{1}{2} \right\rangle, \quad |\bar{u}\rangle : \left| -\frac{1}{2}, -\frac{1}{2} \right\rangle, \quad |d\rangle : \left| \frac{1}{2}, -\frac{1}{2} \right\rangle, \quad |\bar{d}\rangle : \left| \frac{1}{2}, \frac{1}{2} \right\rangle. \quad (22)$$

Based on the quark components of hadrons, the isospin states of the hadrons are shown in Table 6. The isospin amplitudes for typical processes are written as

According to the sPlot technique and based on the above DT fit, the weight $W_s(y)$ of each candidate event is calculated as

$$W_s(y) = \frac{\sum_i V_i F_i(y)}{\sum_i N_j F_j(y) + \sum_k N'_k F'_k(y)}, \quad (29)$$

where the index s denotes the signal, $F_{i(j)}(y)$ are the PDFs of the signal ($i(j) = s$) and backgrounds ($i(j) \neq s$) from BKGI to BGKV with floating yields, $F'_k(y)$ are the PDFs of BKGVI with fixed yields, and $N_{i(j)}$ and N'_k are

Table 6: The quark components and isospin states for different hadrons used in the analysis.

	π^+, b^+, ρ^+, a^+	π^0, b^0, ρ^0, a^0	π^-, b^-, ρ^-, a^-
$I = 1$	$ u\bar{d}\rangle : 1, 1\rangle$	$ \frac{u\bar{u}-d\bar{d}}{\sqrt{2}}\rangle : - 1, 0\rangle$	$ d\bar{u}\rangle : - 1, -1\rangle$
	h, ω, ϕ, f		
$I = 0$	$ (u\bar{u} + d\bar{d}) + g(ss)\rangle : - 0, 0\rangle$		

the corresponding yields for each component. The inverse of covariance matrix V_{ij} is calculated with

$$V_{ij}^{-1} = \sum_{n \in \text{Data}} \frac{F_i(y_n)F_j(y_n)}{(\sum_k N_k F_k(y_n) + \sum_l N'_l F'_l(y_n))^2}, \quad (30)$$

where the summations for indices k and l run over all the components of $F_k(y)$ and $F'_l(y)$ as described above, respectively. The summation for index n runs over all the events in the DT fit.

Based on the sPlot technique, $W_s(y)$ defined in Eq. (29) includes the effects of the backgrounds with the fixed number of events. To take into account these effects, the coefficients c_i are calculated as

$$c_i = \sum_j V_{sj} \nu_{ij}, \quad (31)$$

where the summation runs over the signal and backgrounds from BKG I to BKG V with floating yields in the fit, i represents the different components in the BKG VI, and ν_{ij} is

$$\nu_{ij} = \sum_{n \in \text{Data}} \frac{F'_i(y_n)F_j(y_n)}{(\sum_k N_k F_k(y_n) + \sum_l N'_l F'_l(y_n))^2}. \quad (32)$$

With the obtained $W_s(y)$ and c_i , the x distribution of all candidate events with the weight $W_s(y)$ is the real signal together with the contributions of the peaking background in BKG VI,

$$N_s P_s(x) + \sum_j c_j N'_j P'_j(x), \quad (33)$$

where $P_s(x)$ and $P'_j(x)$ are the x distributions of the signal and the peaking background j in the BKG VI and N_s and N'_j are the corresponding yields obtained from the above 2D fit and MC simulation, respectively.

In practice, the PDF of observing a signal event with the given final kinematic p is written as

$$P_s(p) = \frac{\epsilon_s(p) |M_f(p)|^2 \phi_4(p)}{\int \epsilon_s(p) |M_f(p)|^2 d\Phi_4}, \quad (34)$$

where $\epsilon_s(p)$ is the signal efficiency, $|M_f(p)|^2$ is the differential cross section as discussed in Sec. 5, and $\phi_4(p)$ is the PHSP density. The normalization factor is calculated by MC integration with the PHSP signal MC sample after event selection,

$$\int \epsilon_s(p) |M_f(p)|^2 d\Phi_4 \propto \frac{1}{N_{\text{MC}}} \sum_{i=1}^{N_{\text{MC}}} |M_f(p_i)|^2. \quad (35)$$

where the N_{MC} is the number of events of the PHSP signal MC. According to Eq. (33), the weighted likelihood $\ln L$ is given by

$$f \left[\sum_{i \in \text{Data}} W_s(y_i) \ln P_s(p_i) - \sum_j \sum_{i \in \text{BKG}_j} \omega_j \ln P_s(p_i) \right], \quad (36)$$

where the second term in the bracket is the contribution from the peaking background, which is estimated with the corresponding simulated background MC. The normalization factor ω_j is given by

$$\omega_j = c_j N_{\text{BKG}_j}^{\text{Data}} / N_{\text{BKG}_j}^{\text{MC}}. \quad (37)$$

Here, c_j is obtained from Eq. (31), and $N_{\text{BKG}_j}^{\text{Data}}$ and $N_{\text{BKG}_j}^{\text{MC}}$ are the background yields in data and simulated background events, respectively. The factor f in Eq. (36),

$$f = \frac{\sum_{i \in \text{Data}} W_s(y_i) + \sum_j \omega_j N_{\text{BKG}_j}^{\text{MC}}}{\sum_{i \in \text{Data}} W_s^2(y_i) + \sum_j \omega_j^2 N_{\text{BKG}_j}^{\text{MC}}}, \quad (38)$$

is the global factor to correct the statistical bias in the weighted maximum likelihood fit.

The total likelihood function in this analysis is summed over the two signal channels and three tag modes,

$$\ln L_{\text{total}} = \sum_{i \in \text{tag}} \left(\ln L_i^{\pi^+\pi^-\pi^+\pi^-} + \ln L_i^{\pi^+\pi^-\pi^0\pi^0} \right), \quad (39)$$

and the free parameters are optimized via a maximum likelihood fit using the MINUIT [47] package.

Generally, all the possible intermediate processes including the resonances listed in Table 7 and based on J^{PC} conservation are considered in the fit. The only exception are D^0 decays, where parity conservation is not required. Only processes with a significance greater than 5σ are kept during the fit unless otherwise noted. Here, the significance of a specific amplitude is calculated according to the Wilks's Theorem by comparing the change of log-likelihood ($2\Delta \ln L$) to the expected values from the chi-square distribution ($\chi_{\Delta N_{\text{para}}}^2$) with the number of degrees of freedom (NDF) equal to the change of the numbers of fit parameters (ΔN_{para}). If the significance of the amplitudes containing the isospin vector in the 3π invariant mass spectrum is greater than 5σ , the corresponding isospin partners with significance greater than 3σ are also kept. For the P-vector of the $\pi\pi$ S-wave, only the parameters before the 1st, 2nd poles and $\pi\pi$, KK non-resonant terms are considered, and the others are fixed to zero in the nominal fit. Meanwhile, only those with significance greater than 3σ are kept. We assume the same values of the parameter s_0^{prod} in the P-vector of all $\pi\pi$ S-waves and

Table 7: Resonances considered in this analysis.

	$J^P = 0^+$	$J^P = 0^-$	$J^P = 1^+$	$J^P = 1^-$	$J^P = 2^+$	$J^P = 2^-$
$\pi\pi$	$(\pi\pi)_S$			$\rho(770)$ $\rho(1450)$	$f_2(1270)$	
$\pi\pi\pi$		$\pi(1300)$	$a_1(1260)$ $a_1(1420)$ $a_1(1640)$ $h_1(1170)$	$\omega(782)$ $\phi(1020)$ $\pi_1(1400)$ $\pi_1(1600)$	$a_2(1320)$	$\pi_2(1670)$

fix them to $-5 \text{ GeV}^2/c^4$ since they are insensitive to any choice if $s_0^{\text{prod}} \leq -5 \text{ GeV}^2/c^4$.

To find the optimal solution, the baseline model which contains the processes from Refs. [10, 11] is built up first. Next, starting from the baseline model, the significance of each possible process is tested and the most significant one among those satisfying the significance requirement is added to the current model. This step is repeated until no additional processes can be added. After this, the significances of individual processes in the existing model are tested again and those that do not satisfy the significance requirement are removed. The above steps are repeated until all the processes in the model satisfy the significance requirement and no further ones can be added.

With the nominal amplitude model, the fit fraction (FF) of a specific amplitude i is calculated as

$$\text{FF}_i = \frac{\int |\Lambda_i U_i(p)|^2 d\Phi}{\int |\sum_j \Lambda_j U_j(p)|^2 d\Phi}. \quad (40)$$

The CP -even fraction F_+ is calculated as

$$F_+^f = \frac{\int |A_f^+(p)|^2 d\Phi}{\int |A_f^+(p)|^2 + |A_f^-(p)|^2 d\Phi}, \quad (41)$$

where $A_f^\pm(p) = \frac{1}{\sqrt{2}}[A_f(p) \pm \bar{A}_f(p)]$ is the amplitude of the $D^0 \rightarrow f$ decay in a CP -even or CP -odd state. The FF results of different amplitudes are summarized in Tables 8, 9 and 10. The resonant parameters, masses, and widths of $a_1(1260)$ and $\pi(1300)$ are determined by the parameter scans as shown in Fig. 4. The fit results show large interferences among the dominant intermediate processes $D^0 \rightarrow a_1(1260)\pi$, $D^0 \rightarrow \pi(1300)\pi$, $D^0 \rightarrow \rho(770)\rho(770)$, and $D^0 \rightarrow 2(\pi\pi)_S$. The results for F_+ obtained in this analysis are presented in Table 11, which show good agreement with other measurements. In all above tables, the mean values are obtained based on the output from the MINUIT fit, while the corresponding statistical uncertainties are estimated by the bootstrap method [48] based on data, since the weighted maximum likelihood fit is used, and the statistical uncertainties given by the inverse second derivative of the negative logarithmic likelihood are no longer asymptotically correct [49]. In the bootstrap method, the bootstrap samples are generated by repeatedly resampling the data set with replacement

for thousand times, and both sPlot and amplitude analysis are performed for these samples. The width of the distribution of estimated parameter values is used as estimator for the parameter uncertainty. The comparisons between data and MC projection based on the nominal model for various invariant mass and angle distributions are shown in Figs. 5 and 6. To determine the quality of the fit, the goodness of fit is calculated for the amplitude analysis. Here the adaptive bins (with more than 25 events and the sum of weights greater than 0 in each bin) in five-dimensional PHSP $\{M(\pi^+\pi^+), M(\pi^-\pi^-), \cos\theta_{+,+}, \cos\theta_{-,-}, \phi_{+,+,-,-}\}$ and $\{M(\pi^+\pi^-), M(\pi^0\pi^0), \cos\theta_{+,-}, \cos\theta_{0,0}, \phi_{+,-,00}\}$ are defined for $D^0 \rightarrow \pi^+\pi^-\pi^+\pi^-$ and $D^0 \rightarrow \pi^+\pi^-\pi^0\pi^0$, respectively, where θ is the helicity angle of π in the corresponding $\pi\pi$ system, ϕ is the angle between two $\pi\pi$ decay planes in the D^0 rest frame and the indices $+$, $-$ and 0 in subscript represent π^+ , π^- and π^0 , respectively. The χ^2 of the amplitude analysis fit is calculated as

$$\chi^2 = \sum_i \frac{(w_{\text{Data}}^i - w_{\text{MC}}^i)^2}{(w_{\text{Data}}^i)^2 + (w_{\text{MC}}^i)^2}, \quad (42)$$

where the summation runs over all the bins in the ten variables, w^i and $(w^i)^2$ are the sum and quadrature sum of weights in the i -th bin, respectively. The goodness of fit is calculated to be $\chi^2/\text{NDF} = 382/396 = 0.96$, where NDF is equal to $(N_{\text{bin}} - N_{\text{para}} - 6)$.

7 SYSTEMATIC UNCERTAINTY OF THE AMPLITUDE ANALYSIS

The systematic uncertainties of the amplitude analysis come from two aspects. One is the experimental systematic uncertainty which includes those from background estimation and detection efficiency over PHSP. Another is the model-dependent uncertainty which includes those from resonance line shape, radii of Blatt-Weisskopf barrier factors, quantum correlation parameters, extra amplitudes, and fit bias. To estimate these uncertainties for each source, the fit is performed with alternative conditions, and the deviations from the nominal results are taken as the corresponding uncertainties. Table 12 summarizes the systematic uncertainties on the FFs, resonance parameters, and CP -even fractions in the unit of the statistical uncertainty, where the total system-

Table 8: The fit parameters, FFs and significances of individual amplitudes, where the first uncertainties are statistical and the second in FFs are systematic.

Amplitude	Magnitude	Phase (rad)	FF (%)		Significance (σ)
			$\pi^+\pi^-\pi^+\pi^-$	$\pi^+\pi^-\pi^0\pi^0$	
$a_1(1260)^+\pi^-$	100(fixed)	0(fixed)	$82.2 \pm 3.3 \pm 16.0$	$57.4 \pm 2.7 \pm 7.3$	>20
$a_1(1260)^-\pi^+$	35.3 ± 2.7	0.23 ± 0.07	$10.3 \pm 1.5 \pm 2.5$	$7.2 \pm 1.1 \pm 2.2$	15.6
$a_1(1260)^0\pi^0$	50.9 ± 3.1	-2.99 ± 0.06	-	$32.9 \pm 3.2 \pm 8.6$	>20
$a_1(1420)^+\pi^-$	19.0 ± 3.6	2.70 ± 0.18	$0.6 \pm 0.2 \pm 0.2$	$0.3 \pm 0.1 \pm 0.1$	6.0
$a_1(1640)^+\pi^-$	20.1 ± 3.0	-2.07 ± 0.16	$1.7 \pm 0.5 \pm 0.9$	$1.1 \pm 0.3 \pm 0.7$	7.3
$a_1(1640)^-\pi^+$	10.5 ± 2.8	-1.26 ± 0.29	$0.5 \pm 0.3 \pm 0.3$	$0.3 \pm 0.2 \pm 0.2$	5.2
$a_2(1320)^+\pi^-$	0.23 ± 0.07	-2.92 ± 0.30	$0.2 \pm 0.1 \pm 0.1$	$0.2 \pm 0.1 \pm 0.1$	4.6
$a_2(1320)^-\pi^+$	0.30 ± 0.05	-0.47 ± 0.21	$0.4 \pm 0.1 \pm 0.1$	$0.3 \pm 0.1 \pm 0.1$	6.4
$h_1(1170)^0\pi^0$	9.7 ± 2.2	-0.59 ± 0.27	-	$1.3 \pm 0.6 \pm 1.1$	6.5
$\pi(1300)^+\pi^-$	76.3 ± 3.6	-2.325 ± 0.044	$32.3 \pm 2.6 \pm 4.5$	$15.6 \pm 1.4 \pm 2.6$	>20
$\pi(1300)^-\pi^+$	65.1 ± 3.4	-2.631 ± 0.045	$23.5 \pm 2.3 \pm 4.1$	$11.4 \pm 1.1 \pm 2.2$	19.0
$\pi(1300)^0\pi^0$	61.1 ± 3.2	0.61 ± 0.05	-	$23.2 \pm 2.8 \pm 3.5$	16.8
$\pi_2(1670)^0\pi^0$	12.2 ± 1.5	-1.11 ± 0.14	-	$1.1 \pm 0.2 \pm 0.4$	6.9
$\rho(770)^0\rho(770)^0$	-	-	$28.0 \pm 1.9 \pm 3.2$	-	>20
$\rho(770)^0\rho(770)^0[S]$	6.1 ± 1.1	-3.10 ± 0.17	$1.7 \pm 0.6 \pm 0.5$	-	6.5
$\rho(770)^0\rho(770)^0[P]$	6.17 ± 0.36	1.62 ± 0.07	$9.8 \pm 1.0 \pm 0.9$	-	19.5
$\rho(770)^0\rho(770)^0[D]$	4.54 ± 0.22	-3.06 ± 0.05	$23.1 \pm 2.1 \pm 2.4$	-	>20
$\rho(770)^0\rho(1450)^0$	-	-	$2.5 \pm 0.9 \pm 1.1$	-	8.0
$\rho(770)^0\rho(1450)^0[P]$	13.9 ± 2.5	0.68 ± 0.20	$1.0 \pm 0.4 \pm 0.5$	-	6.4
$\rho(770)^0\rho(1450)^0[D]$	5.6 ± 1.3	3.08 ± 0.20	$1.5 \pm 0.9 \pm 1.1$	-	5.0
$\rho(770)^+\rho(770)^-$	-	-	-	$90.9 \pm 3.9 \pm 7.9$	>20
$\rho(770)^+\rho(770)^-[S]$	13.7 ± 1.2	3.03 ± 0.09	-	$13.0 \pm 2.0 \pm 3.5$	13.0
$\rho(770)^+\rho(770)^-[P]$	7.10 ± 0.36	-1.69 ± 0.07	-	$19.6 \pm 1.3 \pm 2.0$	>20
$\rho(770)^+\rho(770)^-[D]$	4.59 ± 0.22	0.06 ± 0.05	-	$36.0 \pm 3.0 \pm 2.5$	>20
$\rho(770)^+\rho(1450)^-[D]$	8.1 ± 1.7	-1.01 ± 0.18	-	$1.69 \pm 0.8 \pm 1.7$	6.3
$\rho(770)^0(\pi\pi)_S$	-	-	$2.7 \pm 0.6 \pm 1.8$	$1.0 \pm 0.2 \pm 0.4$	12.8
β_1	8.4 ± 3.6	-1.68 ± 0.50	-	-	-
$f_{\pi\pi}^{\text{prod}}$	40.7 ± 5.0	-0.50 ± 0.14	-	-	-
f_{KK}^{prod}	121 ± 25	1.73 ± 0.23	-	-	-
$(\pi^+\pi^-)_S(\pi\pi)_S$	-	-	$62.8 \pm 4.6 \pm 9.6$	$37.4 \pm 3.0 \pm 5.1$	>20
$a_{1,1}$	2224 ± 35	-1.044 ± 0.019	-	-	-
$a_{1,2}$	7287 ± 62	1.727 ± 0.009	-	-	-
$b_{2,\pi\pi}$	8816 ± 120	-1.107 ± 0.014	-	-	-
$c_{[\pi\pi,\pi\pi]}$	2433 ± 96	1.796 ± 0.043	-	-	-
$c_{[\pi\pi, KK]}$	5417 ± 477	2.68 ± 0.10	-	-	-
$f_2(1270)^0(\pi\pi)_S$	-	-	$1.8 \pm 0.4 \pm 1.2$	$1.1 \pm 0.2 \pm 0.8$	9.1
$f_{\pi\pi}^{\text{prod}}$	18.3 ± 1.8	-1.39 ± 0.10	-	-	-
f_{KK}^{prod}	56 ± 10	2.29 ± 0.20	-	-	-
$\omega(782)\pi^0$	1.58 ± 0.30	-0.50 ± 0.44	-	$0.9 \pm 0.4 \pm 0.2$	6.1
$\phi(1020)\pi^0$	0.44 ± 0.06	2.51 ± 0.41	-	$1.5 \pm 0.4 \pm 0.3$	7.4

Table 9: The fit parameters, FFs and significance for the three-body decays of $a_1(1260)$, $a_1(1420)$, $a_1(1640)$, $a_2(1320)$, $h_1(1170)$, $\pi(1300)$ and $\pi_2(1670)$. The first uncertainties are statistical and the second in FFs are systematic.

Amplitude	Magnitude	Phase (rad)	Relative FF (%)			Significance (σ)
			$\pi^+\pi^-\pi^+\pi^-$	$\pi^+\pi^-\pi^0\pi^0$		
			charge = ± 1	charge = ± 1	charge = 0	
$a_1(1260) \rightarrow \rho(770)\pi[S]$	1(fixed)	0(fixed)	$79.7 \pm 2.2 \pm 3.5$	$81.2 \pm 2.0 \pm 3.2$	$78.9 \pm 2.2 \pm 3.8$	>20
$a_1(1260) \rightarrow \rho(770)\pi[D]$	0.060 ± 0.009	-0.01 ± 0.17	$1.3 \pm 0.3 \pm 0.8$	$1.2 \pm 0.3 \pm 0.7$	$1.3 \pm 0.3 \pm 0.8$	7.5
$a_1(1260) \rightarrow f_2(1270)\pi[P]$	0.311 ± 0.033	-1.58 ± 0.11	$1.8 \pm 0.4 \pm 0.6$	$0.8 \pm 0.2 \pm 0.2$	$1.2 \pm 0.2 \pm 0.4$	10.6
$a_1(1260) \rightarrow (\pi^+\pi^-)_S\pi[P]$	-	-	$5.4 \pm 0.6 \pm 1.0$	$3.1 \pm 0.4 \pm 0.8$	$3.9 \pm 0.5 \pm 0.9$	15.8
β_1	0.83 ± 0.13	-2.18 ± 0.14	-	-	-	-
$f_{\pi\pi}^{\text{prod}}$	2.47 ± 0.16	0.34 ± 0.08	-	-	-	-
f_{KK}^{prod}	6.59 ± 0.84	1.76 ± 0.12	-	-	-	-
$\pi(1300) \rightarrow \rho(770)\pi$	1(fixed)	0(fixed)	$53.8 \pm 2.9 \pm 8.8$	$79.0 \pm 2.0 \pm 6.8$	$73.6 \pm 2.6 \pm 8.9$	>20
$\pi(1300) \rightarrow (\pi^+\pi^-)_S\pi$	-	-	$51.1 \pm 2.9 \pm 8.7$	$26.2 \pm 2.1 \pm 6.5$	$36.7 \pm 2.6 \pm 8.6$	14.4
β_1	5.0 ± 0.5	-0.64 ± 0.10	-	-	-	-
f_{KK}^{prod}	43.8 ± 2.8	0.34 ± 0.06	-	-	-	-
$a_1(1420) \rightarrow f_0(980)\pi[P]$	1(fixed)	0(fixed)	100	100	-	6.0
$a_1(1640) \rightarrow \rho(770)\pi[S]$	1(fixed)	0(fixed)	100	100	-	9.1
$a_2(1320) \rightarrow \rho(770)\pi[D]$	1(fixed)	0(fixed)	100	100	-	7.3
$h_1(1170) \rightarrow \rho(770)\pi[S]$	1(fixed)	0(fixed)	-	-	100	6.5
$\pi_2(1670) \rightarrow f_2(1270)\pi[S]$	1(fixed)	0(fixed)	-	-	100	6.9

Table 10: Masses and widths of $a_1(1260)$ and $\pi(1300)$ obtained via parameter scans and presented in the PDG [23].

	This work		PDG	
	Mass (GeV/c^2)	Width (GeV)	Mass (GeV/c^2)	Width (GeV)
$a_1(1260)$	$1.193 \pm 0.005 \pm 0.023$	$0.487 \pm 0.009 \pm 0.041$	1.230 ± 0.040	$0.250 - 0.600$
$\pi(1300)$	$1.534 \pm 0.011 \pm 0.022$	$0.610 \pm 0.030 \pm 0.093$	1.300 ± 0.100	$0.200 - 0.600$

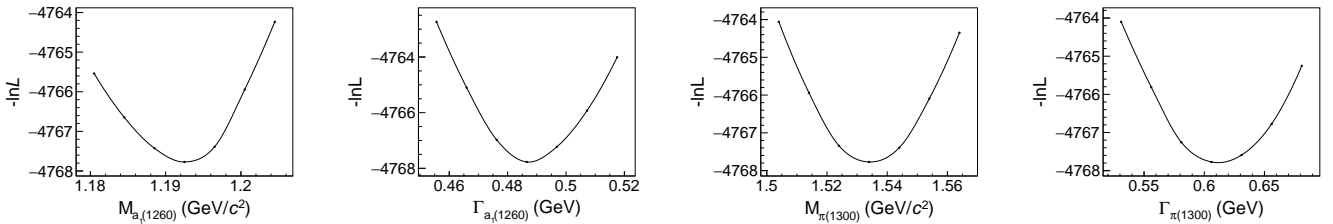


Figure 4: Likelihood scans for masses and widths of $a_1(1260)$ and $\pi(1300)$.

Table 11: The CP -even fractions obtained in this work and comparisons with the CLEO-c and prior BESIII measurements.

	$F_+^{\pi^+\pi^-\pi^+\pi^-}$	$F_+^{\pi^+\pi^-\pi^0\pi^0} (\text{non-}\eta)$
This work (model-dependent)	$(75.2 \pm 1.1_{\text{stat.}} \pm 1.5_{\text{syst.}})\%$	$(68.9 \pm 1.5_{\text{stat.}} \pm 2.4_{\text{syst.}})\%$
CLEO-c (model-dependent)	$(72.9 \pm 0.9_{\text{stat.}} \pm 1.5_{\text{syst.}} \pm 1.0_{\text{model}})\%$ [11]	-
CLEO-c (model-independent, global)	$(73.7 \pm 2.8)\%$ [50]	-
CLEO-c (model-independent, binned)	$(76.9 \pm 2.1_{\text{stat.}} \pm 1.0_{\text{syst.}} \pm 0.2_{K_S \text{ veto}})\%$ [6]	-
BESIII (model-independent, global)	$(73.4 \pm 1.5_{\text{stat.}} \pm 0.8_{\text{syst.}})\%$ [51]	$(68.2 \pm 7.7)\%$ [52]

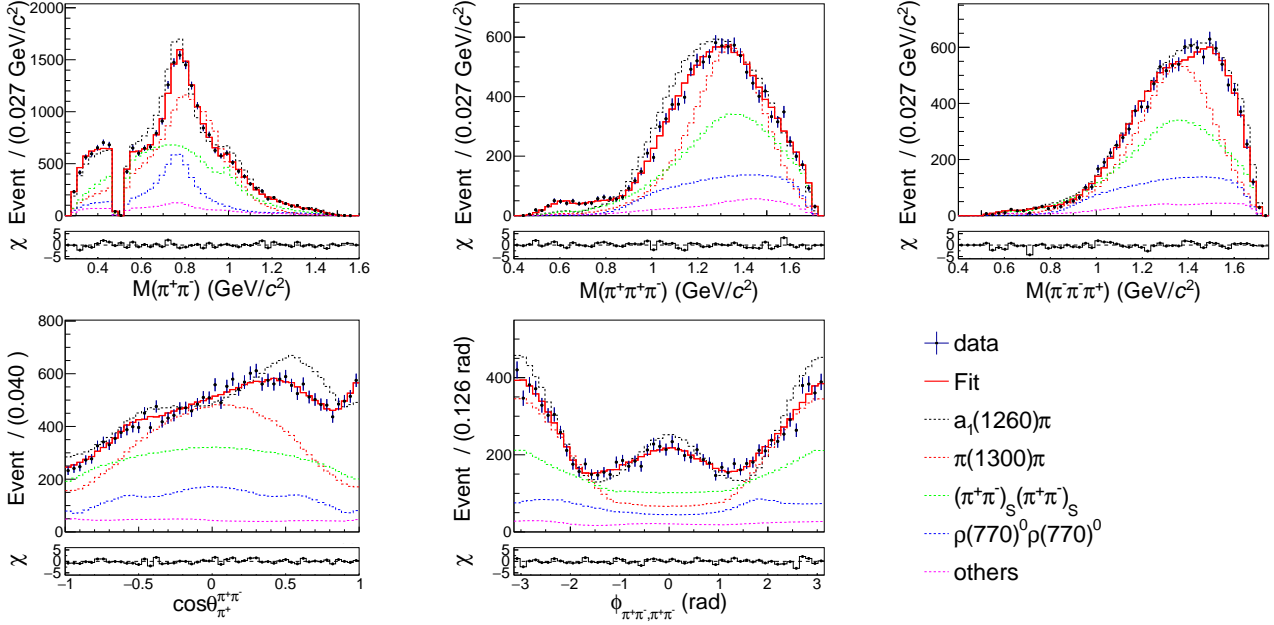


Figure 5: The mass and angular distributions for $D^0 \rightarrow \pi^+\pi^-\pi^+\pi^-$, where θ_a^{ab} is the helicity angle of a in the ab system, $\phi_{ab,cd}$ is the angle between the decay planes of ab and cd systems in the D^0 rest frame.

atic uncertainties are the square roots of the quadrature sums of the individual contributions. The individual uncertainties are obtained as follows.

- Background estimation

The sPlot technique is used to estimate the signal weight and background, the corresponding sources of systematic uncertainty are all the PDFs and the magnitudes of peaking backgrounds in BKGVI in the 2D fit on the M_{bc}^{tag} versus M_{bc}^{sig} distribution. To estimate the corresponding uncertainties, an alternative fit on the M_{bc}^{tag} versus M_{bc}^{sig} distribution is performed by varying the means and widths of two Gaussian functions by $\pm 1\sigma$ for signal, varying the fixed parameters of the ARGUS function by $\pm 1\sigma$ for BKG I and BKG II, changing the Student's function to the bifurcated Student's function with different n and σ on the left and right sides of the maximum value and two ARGUS functions to one ARGUS function on the $(M_{bc}^{\text{sig}} + M_{bc}^{\text{tag}})$ dimension for BKG III, varying the means and widths of the bifurcated Gaussian functions by $\pm 1\sigma$ for BKG IV and BKG V and varying the fixed peaking background yields by $\pm 1\sigma$. The output results are used in the sPlot technique and amplitude analysis.

- Detection efficiency

The systematic uncertainties due to detection efficiencies are from the π^\pm tracking/PID and π^0 reconstruction. The corresponding uncertainties are obtained by weighting the PHSP signal MC sample with a factor $\epsilon_{\text{Data}}/\epsilon_{\text{MC}}$ when normalizing the PDF in the amplitude analysis, where ϵ_{Data} and ϵ_{MC} are the efficiencies of data and MC simulation, respectively. The π^\pm tracking/PID efficiencies are quoted from Ref. [53], while the efficiency of the π^0 reconstruction is studied with the control samples

of $D^0 \rightarrow K^-\pi^+\pi^0$ and $D^0 \rightarrow \pi^+\pi^-\pi^0$ versus three tag modes used in this analysis.

- The parameters and models of resonances

The systematic uncertainties associated with the masses and widths of resonances in the amplitude analysis are estimated by shifting the corresponding fixed PDG [23] values or optimized values by $\pm 1\sigma$. The systematic uncertainties associated with the model of $\pi\pi$ S-wave are estimated by replacing the K-matrix formula with the sum of three independent resonances of $f_0(500)$, $f_0(980)$, and $f_0(1370)$, which are described with the formula in Ref. [54], a Flatté parametrization, and a relative Breit-Wigner function with energy dependent width. The overall uncertainties are the square roots of the quadrature sums of the individual contributions.

- Radii of Blatt-Weisskopf barrier factors

The systematic uncertainties due to radii of Blatt-Weisskopf barrier factors are obtained by varying the radii of the D^0 meson and other resonances by $\pm 1 \text{ GeV}^{-1}c$ in the amplitude analysis, and the square root of the quadrature sum of the individual effects is taken as the uncertainty.

- Quantum correlation correction

The systematic uncertainty due to the quantum correlation correction is estimated by varying the input quantum correlation parameters by $\pm 1\sigma$ in the amplitude analysis.

- Extra amplitudes

The systematic uncertainties due to the extra amplitudes are estimated with the alternative fits with the models including an additional amplitude of $f_2(1270)f_2(1270)[D]$ or

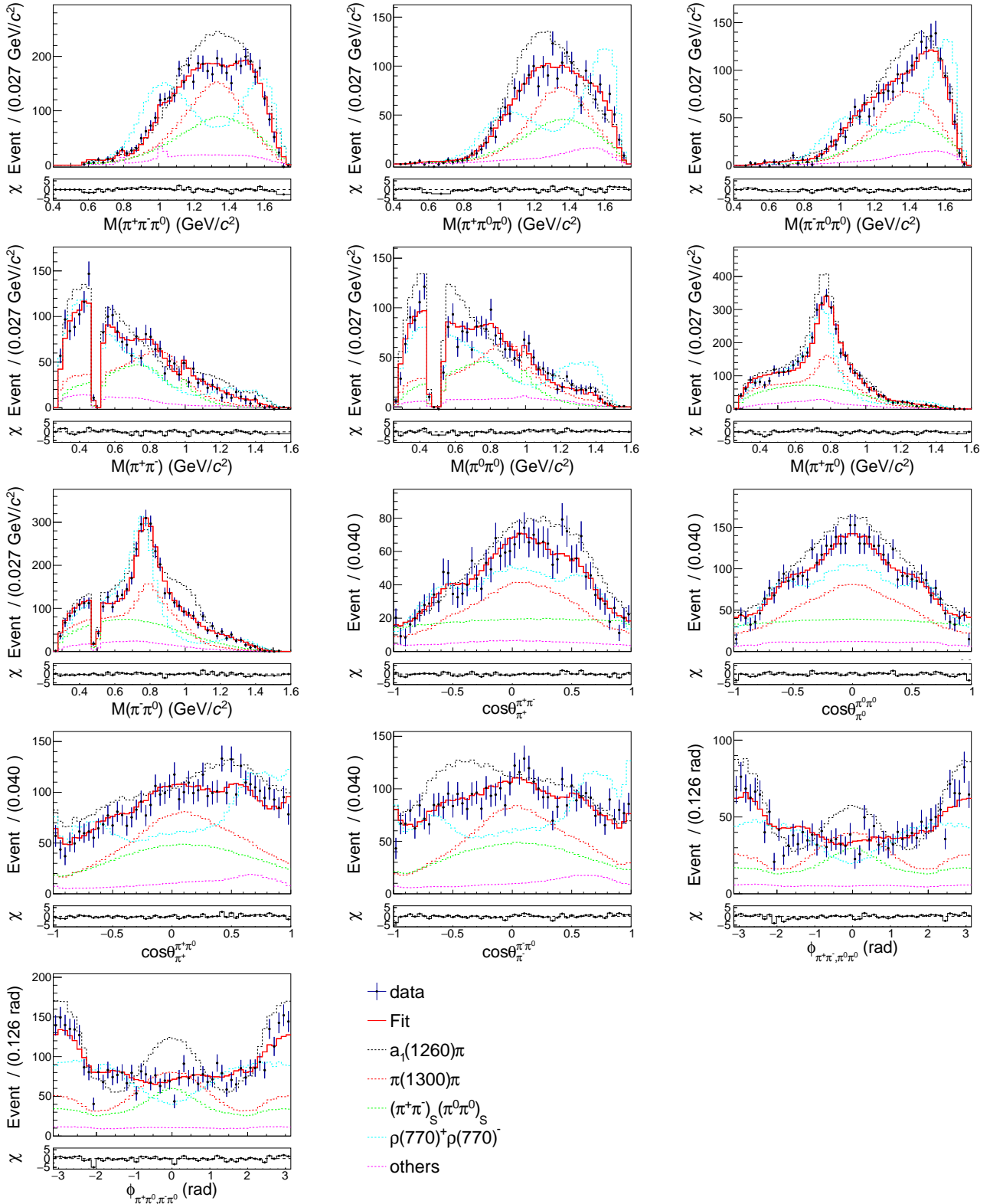


Figure 6: The mass and angular distributions in $D^0 \rightarrow \pi^+\pi^-\pi^+\pi^-$, where θ_{ab} is the helicity angle of a in the ab system and $\phi_{ab,cd}$ is the angle between the decay planes of ab and cd systems in the D^0 rest frame.

$1^{++}[\rho(770)^+\pi^-[S]]_{\text{NR}}\pi^0$ (“NR” represents non-resonant contribution), which are of 3σ to 5σ significance based on the nominal model. The square root of the quadrature sum of the individual effects is taken as the uncertainty.

- Fit bias

The sPlot technique, MC integration, detection resolution, and many other potential problems from fit tools may lead to fit bias. To estimate this fit bias, 100 sets of samples with the same size and signal purity as the data are generated, where the signal events are generated according to the nominal model and the background events are from the in-

clusive MC sample. The amplitude fit is performed on these samples, and the average deviations of the fitted parameters from their input values are taken as uncertainties due to fit bias.

8 MEASUREMENT OF BRANCHING FRACTIONS

The absolute branching fractions of $D^0 \rightarrow \pi^+\pi^-\pi^+\pi^-$ and $D^0 \rightarrow \pi^+\pi^-\pi^0\pi^0$ (non- η) are measured with the DT method. The numbers of ST events (N_g^{ST}) for the tag mode g and DT events (N_{fg}^{DT}) for the self-conjugated signal model f with the tag mode g are given by

$$N_g^{\text{ST}} = 2N_{D^0\bar{D}^0}\mathcal{B}_g\epsilon_g^{\text{ST}}(1+y_D^2)(1+r_g^2-2r_gR_gy_D\cos\delta_g), \quad (43)$$

$$N_{fg}^{\text{DT}} = 2N_{D^0\bar{D}^0}\mathcal{B}_f\mathcal{B}_g\epsilon_{fg}^{\text{DT}}(1+y_D^2)[1+r_g^2-2r_gR_g\cos\delta_g(2F_+^f-1)]. \quad (44)$$

Here, $N_{D^0\bar{D}^0}$ is the total number of $D^0\bar{D}^0$ pairs in data, \mathcal{B}_f and \mathcal{B}_g are the branching fractions of the signal mode f and tag mode g , respectively, ϵ_f^{ST} and $\epsilon_{fg}^{\text{DT}}$ are the corresponding ST and DT efficiencies, and y_D is the D^0 - \bar{D}^0 mixing parameter. By combining Eqs. (43) and (44) and ignoring the term $2r_gR_gy_D\cos\delta_g$ in Eq. (43), the branching fraction of $D^0 \rightarrow f$ is given by

$$\mathcal{B}_f = \frac{\sum_g N_{fg}^{\text{DT}}}{\sum_g N_g^{\text{ST}}(\epsilon_{fg}^{\text{DT}}/\epsilon_g^{\text{ST}}) \left[1 - \frac{2r_gR_g\cos\delta_g}{1+r_g^2}(2F_+^f-1) \right]}. \quad (45)$$

As described in Sec. 4, the ST and DT yields are extracted by performing an unbinned maximum likelihood fit on the $M_{\text{bc}}^{\text{tag}}$ distribution and the 2D distribution of $M_{\text{bc}}^{\text{tag}}$ versus $M_{\text{bc}}^{\text{sig}}$, respectively. The corresponding ST and DT efficiencies are obtained with the similar fit processes on the signal MC sample as described in Sec. 2. The corresponding ST and DT yields as well as the ST and DT efficiencies are summarized in Table 3. According to Eq. (45) and the values in Table 3, the branching fractions of $D^0 \rightarrow \pi^+\pi^-\pi^+\pi^-$ and $D^0 \rightarrow \pi^+\pi^-\pi^0\pi^0$ (non- η) are calculated and summarized in Table 13. According to the FFs obtained in the amplitude analysis, the branching fractions of the intermediate processes are also determined. The obtained results are summarized in Table 14.

Benefiting from the DT method, most of the systematic uncertainties associated with the ST selection are cancelled. The relative systematic uncertainties in the branching fraction measurement are summarized in Table 15, where the total uncertainties are the square roots of the quadrature sums of the individual ones. Details of the systematic uncertainties in the branching fraction measurements are described below.

- Tracking efficiency

The tracking efficiency of π^\pm has been studied in Ref. [53]. The systematic uncertainties are assigned

by re-weighting the data-MC difference in π^\pm tracking efficiencies according to the momentum distribution of π^\pm in the signal MC sample. They are assigned to be 0.4% and 0.2% for $D^0 \rightarrow \pi^+\pi^-\pi^+\pi^-$ and $D^0 \rightarrow \pi^+\pi^-\pi^0\pi^0$, respectively.

- PID efficiency

The PID efficiency of π^\pm has been studied in Ref. [53]. The systematic uncertainties are assigned by re-weighting the data-MC difference in π^\pm PID efficiencies according to the momentum distribution of π^\pm in the signal MC sample. They are assigned to be 1.2% and 0.6% for $D^0 \rightarrow \pi^+\pi^-\pi^+\pi^-$ and $D^0 \rightarrow \pi^+\pi^-\pi^0\pi^0$, respectively.

- π^0 reconstruction efficiency

The π^0 reconstruction efficiency is studied by the control samples $\bar{D}^0 \rightarrow K^+\pi^-$, $K^+\pi^-\pi^0$, $K^+\pi^-\pi^+\pi^-$ versus $D^0 \rightarrow K^-\pi^+\pi^0$, $\pi^+\pi^-\pi^0$. The corresponding systematic uncertainty for $D^0 \rightarrow \pi^+\pi^-\pi^0\pi^0$ is assigned to be 1.3%, by re-weighting the data-MC difference in π^0 reconstruction efficiencies according to the momentum distribution of π^0 in the signal MC sample.

- ΔE requirement in signal side

To study the systematic uncertainty from the ΔE requirement of the signal side, the ΔE of the signal MC sample is smeared by a Gaussian function, while the mean and width are obtained by performing a fit to the ΔE distribution of data with the signal MC shape convolved with a Gaussian function. The resultant changes of the efficiencies with respect to the nominal values, 0.1% for both $D^0 \rightarrow \pi^+\pi^-\pi^+\pi^-$ and $D^0 \rightarrow \pi^+\pi^-\pi^0\pi^0$, are taken as the systematic uncertainties.

- ST fit

Table 12: Systematic uncertainties in the FFs, resonance parameters and CP -even fractions in units of statistical standard deviations. 1: Background estimation. 2: Detection efficiency. 3: Resonance parameters. 4: Radii of Blatt-Weisskopf barrier factors. 5: Quantum correlation correction. 6: Extra amplitudes. 7: Fit bias. For the items with “/”, the quantities before and after “/” are for $D^0 \rightarrow \pi^+\pi^-\pi^+\pi^-$ and $D^0 \rightarrow \pi^+\pi^-\pi^0\pi^0$, respectively.

	1	2	3	4	5	6	7	Total
FF($D^0 \rightarrow a_1(1260)^+\pi^-$)	0.6/1.1	0.0/0.1	3.8/0.5	3.0/2.1	0.0/0.1	0.2/1.1	0.3/0.1	4.9/2.7
FF($D^0 \rightarrow a_1(1260)^-\pi^+$)	0.1/0.1	0.1/0.1	0.7/1.5	1.4/1.2	0.1/0.1	0.7/0.7	0.2/0.2	1.7/2.1
FF($D^0 \rightarrow a_1(1260)^0\pi^0$)	-/0.4	-/0.1	-/1.8	-/1.7	-/0.0	-/0.9	-/0.2	-/2.6
FF($D^0 \rightarrow a_1(1420)^+\pi^-$)	0.1/0.2	0.0/0.0	0.4/0.7	0.4/0.5	0.0/0.1	0.6/0.5	0.1/0.0	0.8/1.0
FF($D^0 \rightarrow a_1(1640)^+\pi^-$)	0.7/0.8	0.2/0.2	0.6/0.9	1.1/1.1	0.2/0.2	1.2/1.3	0.2/0.1	1.9/2.1
FF($D^0 \rightarrow a_1(1640)^-\pi^+$)	0.1/0.1	0.1/0.1	0.4/0.2	0.6/0.6	0.2/0.2	0.9/1.0	0.0/0.0	1.2/1.2
FF($D^0 \rightarrow a_2(1320)^+\pi^-$)	0.1/0.2	0.2/0.2	0.5/0.4	0.2/0.1	0.1/0.1	0.3/0.2	0.3/0.3	0.7/0.6
FF($D^0 \rightarrow a_2(1320)^-\pi^+$)	0.1/0.0	0.0/0.0	0.7/0.3	0.5/0.6	0.1/0.1	0.4/0.5	0.1/0.1	1.0/0.9
FF($D^0 \rightarrow h_1(1170)^0\pi^0$)	-/0.7	-/0.1	-/1.1	-/0.7	-/0.0	-/1.0	-/0.2	-/1.8
FF($D^0 \rightarrow \pi(1300)^+\pi^-$)	0.6/0.9	0.1/0.1	0.9/1.0	1.1/1.2	0.2/0.1	0.6/0.2	0.0/0.0	1.7/1.8
FF($D^0 \rightarrow \pi(1300)^-\pi^+$)	0.1/0.4	0.2/0.2	1.1/1.4	1.2/1.5	0.1/0.1	0.5/0.1	0.0/0.1	1.8/2.1
FF($D^0 \rightarrow \pi(1300)^0\pi^0$)	-/0.5	-/0.2	-/0.9	-/0.6	-/0.0	-/0.2	-/0.0	-/1.2
FF($D^0 \rightarrow \pi_2(1670)^0\pi^0$)	-/0.8	-/0.1	-/0.3	-/0.4	-/0.1	-/1.4	-/0.1	-/1.7
FF($D^0 \rightarrow \rho(770)^0\rho(770)^0$)	0.3/-	0.0/-	1.5/-	0.2/-	0.1/-	0.6/-	0.0/-	1.7/-
FF($D^0 \rightarrow \rho(770)^0\rho(770)^0[S]$)	0.1/-	0.0/-	0.7/-	0.3/-	0.1/-	0.3/-	0.1/-	0.8/-
FF($D^0 \rightarrow \rho(770)^0\rho(770)^0[P]$)	0.0/-	0.0/-	0.5/-	0.5/-	0.3/-	0.1/-	0.4/-	0.9/-
FF($D^0 \rightarrow \rho(770)^0\rho(770)^0[D]$)	0.3/-	0.0/-	0.9/-	0.3/-	0.1/-	0.5/-	0.2/-	1.1/-
FF($D^0 \rightarrow \rho(770)^0\rho(1450)^0$)	0.0/-	0.0/-	0.7/-	0.7/-	0.1/-	0.8/-	0.0/-	1.2/-
FF($D^0 \rightarrow \rho(770)^0\rho(1450)^0[P]$)	0.1/-	0.2/-	1.3/-	0.6/-	0.3/-	0.1/-	0.2/-	1.5/-
FF($D^0 \rightarrow \rho(770)^0\rho(1450)^0[D]$)	0.1/-	0.1/-	0.2/-	0.9/-	0.1/-	0.8/-	0.1/-	1.2/-
FF($D^0 \rightarrow \rho(770)^+\rho(770)^-$)	-/0.9	-/0.0	-/1.3	-/0.5	-/0.1	-/1.0	-/0.3	-/2.0
FF($D^0 \rightarrow \rho(770)^+\rho(770)^-[S]$)	-/0.6	-/0.1	-/1.1	-/0.6	-/0.0	-/1.0	-/0.1	-/1.7
FF($D^0 \rightarrow \rho(770)^+\rho(770)^-[P]$)	-/1.0	-/0.2	-/0.5	-/0.4	-/0.1	-/0.8	-/0.1	-/1.5
FF($D^0 \rightarrow \rho(770)^+\rho(770)^-[D]$)	-/0.1	-/0.1	-/0.4	-/0.3	-/0.1	-/0.6	-/0.2	-/0.8
FF($D^0 \rightarrow \rho(770)^+\rho(1450)^-[D]$)	-/0.7	-/0.1	-/1.9	-/0.8	-/0.1	-/0.7	-/0.4	-/2.3
FF($D^0 \rightarrow \rho(770)^0(\pi\pi)_S$)	0.5/0.3	0.0/0.0	2.7/1.8	0.1/0.1	0.0/0.0	1.0/0.7	0.2/0.2	3.0/2.0
FF($D^0 \rightarrow (\pi^+\pi^-)_S(\pi\pi)_S$)	0.1/0.6	0.0/0.0	2.0/1.3	0.6/0.8	0.1/0.0	0.3/0.5	0.1/0.2	2.1/1.7
FF($D^0 \rightarrow f_2(1270)^0(\pi\pi)_S$)	0.0/0.1	0.0/0.0	2.6/2.9	1.1/1.0	0.0/0.0	1.4/1.6	0.1/0.1	3.1/3.5
FF($D^0 \rightarrow \omega(782)\pi^0$)	-/0.1	-/0.0	-/0.3	-/0.1	-/0.0	-/0.4	-/0.1	-/0.5
FF($D^0 \rightarrow \phi(1020)\pi^0$)	-/0.2	-/0.1	-/0.3	-/0.2	-/0.1	-/0.5	-/0.4	-/0.8
FF($a_1(1260)^\pm \rightarrow \rho(770)\pi[S]$)	0.8/0.8	0.1/0.1	1.2/1.2	0.4/0.4	0.1/0.1	0.6/0.6	0.1/0.0	1.6/1.6
FF($a_1(1260)^\pm \rightarrow \rho(770)\pi[D]$)	0.1/0.1	0.0/0.0	2.2/2.1	0.5/0.4	0.0/0.0	0.1/0.1	0.2/0.2	2.2/2.2
FF($a_1(1260)^\pm \rightarrow f_2(1270)\pi[P]$)	0.7/0.7	0.0/0.0	0.4/0.3	1.2/1.2	0.1/0.1	0.3/0.3	0.1/0.1	1.5/1.5
FF($a_1(1260)^\pm \rightarrow (\pi^+\pi^-)_S\pi[P]$)	0.8/0.9	0.1/0.0	1.0/1.6	0.3/0.1	0.2/0.1	0.9/0.8	0.2/0.2	1.6/2.0
FF($a_1(1260)^0 \rightarrow \rho(770)\pi[S]$)	-/0.7	-/0.1	-/1.4	-/0.3	-/0.1	-/0.6	-/0.0	-/1.7
FF($a_1(1260)^0 \rightarrow \rho(770)\pi[D]$)	-/0.1	-/0.0	-/2.2	-/0.4	-/0.0	-/0.1	-/0.2	-/2.2
FF($a_1(1260)^0 \rightarrow f_2(1270)\pi[P]$)	-/0.7	-/0.0	-/0.4	-/1.4	-/0.1	-/0.3	-/0.1	-/1.7
FF($a_1(1260)^0 \rightarrow (\pi^+\pi^-)_S\pi[P]$)	-/0.8	-/0.0	-/1.6	-/0.1	-/0.1	-/0.8	-/0.3	-/2.0
FF($\pi(1300)^\pm \rightarrow \rho(770)\pi$)	0.0/0.2	0.1/0.1	2.0/0.8	2.2/3.3	0.1/0.1	0.4/0.3	0.3/0.3	3.1/3.4
FF($\pi(1300)^\pm \rightarrow (\pi^+\pi^-)_S\pi$)	0.1/0.1	0.1/0.1	1.8/1.2	2.3/2.9	0.1/0.1	0.3/0.2	0.3/0.4	3.0/3.1
FF($\pi(1300)^0 \rightarrow \rho(770)\pi$)	-/0.2	-/0.1	-/1.0	-/3.3	-/0.1	-/0.4	-/0.2	-/3.5
FF($\pi(1300)^0 \rightarrow (\pi^+\pi^-)_S\pi$)	-/0.0	-/0.1	-/1.9	-/2.6	-/0.1	-/0.1	-/0.4	-/3.3
$M_{a_1(1260)}$	0.5	0.1	4.0	1.2	0.1	1.6	0.0	4.5
$\Gamma_{a_1(1260)}$	1.7	0.2	3.2	2.3	0.4	1.7	0.0	4.6
$M_{\pi(1300)}$	0.8	0.1	1.1	1.1	0.0	1.0	0.0	2.0
$\Gamma_{\pi(1300)}$	0.7	0.1	2.9	0.4	0.2	0.5	0.0	3.1
F^+	0.7/1.0	0.0/0.2	0.7/0.8	0.3/0.8	0.1/0.1	1.0/0.6	0.1/0.1	1.4/1.6

Table 13: Branching fractions of $D^0 \rightarrow \pi^+\pi^-\pi^+\pi^-$ and $D^0 \rightarrow \pi^+\pi^-\pi^0\pi^0$ (non- η) from this work compared to PDG [23] values, where the first uncertainties are statistical and the second systematic.

	This work	PDG
$D^0 \rightarrow \pi^+\pi^-\pi^+\pi^-$	$(0.688 \pm 0.010 \pm 0.010)\%$	$(0.756 \pm 0.020)\%$
$D^0 \rightarrow \pi^+\pi^-\pi^0\pi^0$ (non- η)	$(0.951 \pm 0.025 \pm 0.021)\%$	$(1.005 \pm 0.090)\%$

Table 14: Branching fractions of the intermediate processes with FFs > 1% in $D^0 \rightarrow \pi^+\pi^-\pi^+\pi^-$ and $D^0 \rightarrow \pi^+\pi^-\pi^0\pi^0$.

Component	Branching fraction (%)	
	$\pi^+\pi^-\pi^+\pi^-$	$\pi^+\pi^-\pi^0\pi^0$
$D^0 \rightarrow a_1(1260)^+\pi^-$	$0.566 \pm 0.024 \pm 0.110$	$0.546 \pm 0.027 \pm 0.070$
$D^0 \rightarrow a_1(1260)^-\pi^+$	$0.071 \pm 0.010 \pm 0.017$	$0.068 \pm 0.011 \pm 0.021$
$D^0 \rightarrow a_1(1260)^0\pi^0$	-	$0.313 \pm 0.031 \pm 0.082$
$D^0 \rightarrow a_1(1640)^+\pi^-$	$0.012 \pm 0.003 \pm 0.006$	$0.010 \pm 0.003 \pm 0.007$
$D^0 \rightarrow h_1(1170)^0\pi^0$	-	$0.012 \pm 0.006 \pm 0.010$
$D^0 \rightarrow \pi(1300)^+\pi^-$	$0.222 \pm 0.018 \pm 0.031$	$0.148 \pm 0.014 \pm 0.025$
$D^0 \rightarrow \pi(1300)^-\pi^+$	$0.162 \pm 0.016 \pm 0.028$	$0.108 \pm 0.011 \pm 0.021$
$D^0 \rightarrow \pi(1300)^0\pi^0$	-	$0.221 \pm 0.027 \pm 0.034$
$D^0 \rightarrow \pi_2(1670)^0\pi^0$	-	$0.010 \pm 0.002 \pm 0.004$
$D^0 \rightarrow \rho(770)^0\rho(770)^0$	$0.193 \pm 0.013 \pm 0.022$	-
$D^0 \rightarrow \rho(770)^0\rho(770)^0[S]$	$0.012 \pm 0.004 \pm 0.003$	-
$D^0 \rightarrow \rho(770)^0\rho(770)^0[P]$	$0.067 \pm 0.007 \pm 0.006$	-
$D^0 \rightarrow \rho(770)^0\rho(770)^0[D]$	$0.159 \pm 0.015 \pm 0.017$	-
$D^0 \rightarrow \rho(770)^0\rho(1450)^0$	$0.017 \pm 0.006 \pm 0.008$	-
$D^0 \rightarrow \rho(770)^0\rho(1450)^0[P]$	$0.007 \pm 0.003 \pm 0.003$	-
$D^0 \rightarrow \rho(770)^0\rho(1450)^0[D]$	$0.010 \pm 0.006 \pm 0.008$	-
$D^0 \rightarrow \rho(770)^+\rho(770)^-$	-	$0.864 \pm 0.040 \pm 0.077$
$D^0 \rightarrow \rho(770)^+\rho(770)^-[S]$	-	$0.124 \pm 0.019 \pm 0.033$
$D^0 \rightarrow \rho(770)^+\rho(770)^-[P]$	-	$0.186 \pm 0.013 \pm 0.019$
$D^0 \rightarrow \rho(770)^+\rho(770)^-[D]$	-	$0.342 \pm 0.029 \pm 0.025$
$D^0 \rightarrow \rho(770)^+\rho(1450)^-[D]$	-	$0.016 \pm 0.008 \pm 0.016$
$D^0 \rightarrow \rho(770)^0(\pi\pi)_S$	$0.019 \pm 0.004 \pm 0.012$	$0.010 \pm 0.002 \pm 0.004$
$D^0 \rightarrow (\pi^+\pi^-)_S(\pi\pi)_S$	$0.432 \pm 0.032 \pm 0.066$	$0.356 \pm 0.029 \pm 0.049$
$D^0 \rightarrow f_2(1270)^0(\pi\pi)_S$	$0.012 \pm 0.003 \pm 0.008$	$0.010 \pm 0.002 \pm 0.008$
$D^0 \rightarrow \omega(782)\pi^0$	-	$0.009 \pm 0.004 \pm 0.002$
$D^0 \rightarrow \phi(1020)\pi^0$	-	$0.014 \pm 0.004 \pm 0.003$

The systematic uncertainty of the ST fit is studied by changing fit range, signal shape and background shape. The fit range is enlarged by $0.005 \text{ GeV}/c^2$. The signal shape is changed by replacing the Gaussian resolution with a Crystal Ball function [55]. The background shape is changed with a floating cut-off parameter for the ARGUS function. The square root of the quadrature sum of the relative change of ST yields, which gives 0.5%, is taken as the systematic uncertainty.

- DT fit

As described in Sec. 7, the systematic uncertainties of the DT fit are obtained by varying the signal and background shapes, and the yields of peaking backgrounds in BKGVI in the fit. The square roots of the quadrature sums of the relative changes of DT yields in the individual changes are 0.6% and 1.4% for $D^0 \rightarrow \pi^+\pi^-\pi^+\pi^-$ and $D^0 \rightarrow \pi^+\pi^-\pi^0\pi^0$, respectively, which are taken as the systematic uncertainties.

- Amplitude model

The DT efficiencies are obtained by varying the parameters of the amplitude model within their uncertainties. The resultant standard deviations of DT efficiencies, which are 0.3% and 0.6% for $D^0 \rightarrow \pi^+\pi^-\pi^+\pi^-$ and $D^0 \rightarrow \pi^+\pi^-\pi^0\pi^0$, respectively, are taken as the systematic uncertainties.

- Quantum correlation corrections

The uncertainties associated with the input parameters of quantum correlation (r , R , δ , and F_+) are 0.3% and 0.4% for $D^0 \rightarrow \pi^+\pi^-\pi^+\pi^-$ and $D^0 \rightarrow \pi^+\pi^-\pi^0\pi^0$, respectively, which are assigned according to uncertainty propagation.

- MC statistics

The systematic uncertainties related with the limited statistics of the signal MC samples are 0.1% and 0.2% for $D^0 \rightarrow \pi^+\pi^-\pi^+\pi^-$ and $D^0 \rightarrow \pi^+\pi^-\pi^0\pi^0$, respectively.

9 SUMMARY

Using 2.93 fb^{-1} of e^+e^- collision data taken at $\sqrt{s} = 3.773 \text{ GeV}$ with the BESIII detector, a joint amplitude analysis of $D^0 \rightarrow \pi^+\pi^-\pi^+\pi^-$ and $D^0 \rightarrow \pi^+\pi^-\pi^0\pi^0(\text{non-}\eta)$ is performed. Large interferences between the dominant amplitudes of $D^0 \rightarrow a_1(1260)\pi$, $D^0 \rightarrow \pi(1300)\pi$, $D^0 \rightarrow \rho(770)\rho(770)$ and $D^0 \rightarrow 2(\pi\pi)_S$ are observed. Based on the amplitude model, the model dependent CP -even fractions of $D^0 \rightarrow \pi^+\pi^-\pi^+\pi^-$ and $D^0 \rightarrow \pi^+\pi^-\pi^0\pi^0(\text{non-}\eta)$ are determined to be $(75.2 \pm 1.1_{\text{stat.}} \pm 1.5_{\text{syst.}})\%$ and $(68.9 \pm 1.5_{\text{stat.}} \pm 2.4_{\text{syst.}})\%$, respectively, which are consistent with the previous measurements carried out by the CLEO [6, 11, 50] and BESIII [51, 52] collaboration. The branching fractions of $D^0 \rightarrow \pi^+\pi^-\pi^+\pi^-$ and $D^0 \rightarrow \pi^+\pi^-\pi^0\pi^0(\text{non-}\eta)$ are measured to be $(0.688 \pm 0.010_{\text{stat.}} \pm 0.010_{\text{syst.}})\%$ and $(0.951 \pm 0.025_{\text{stat.}} \pm 0.021_{\text{syst.}})\%$, respectively, where the former one is 3σ lower than the PDG [23] value. This 3σ deviation may be due to the differences in the amplitude models which affect the global reconstruction efficiency. These results provide essential information for search of CP violation [7] and measurements of the binned strong phase parameter [6], which are important inputs in the γ measurement via the $B^- \rightarrow DK^-$ decay.

The BESIII Collaboration thanks the staff of BEPCII, the IHEP computing center and the supercomputing center of the University of Science and Technology of China (USTC) for their strong support.

Table 15: Relative systematic uncertainties (%) of the measured branching fractions.

Source	$\mathcal{B}(D^0 \rightarrow \pi^+\pi^-\pi^+\pi^-)$	$\mathcal{B}(D^0 \rightarrow \pi^+\pi^-\pi^0\pi^0)$
π^\pm tracking	0.4	0.2
π^\pm PID	1.2	0.6
π^0 reconstruction	-	1.3
ΔE cut in signal side	0.1	0.1
ST fit	0.5	0.5
DT fit	0.6	1.4
Amplitude model	0.3	0.6
Quantum correlation correction	0.3	0.4
MC statistics	0.1	0.2
Total	1.5	2.2

References

- 1 Cabibbo, N., Phys. Rev. Lett. **10** (1963) 531.
- 2 Kobayashi, M. and Maskawa, T., Prog. Theor. Phys. **49** (1973) 652.
- 3 Gronau, M. and Wyler, D., Phys. Lett. B **265** (1991) 172.
- 4 Atwood, D., Dunietz, I., and Soni, A., Phys. Rev. Lett. **78** (1997) 3257.
- 5 Giri, A., Grossman, Y., Soffer, A., and Zupan, J., Phys. Rev. D **68** (2003) 054018.
- 6 Harnew, S., Naik, P., Prouve, C., Rademacker, J., and Asner, D., JHEP **01** (2018) 144.
- 7 Aaij, R. et al., Phys. Lett. B **769** (2017) 345.
- 8 Cheng, H.-Y., Phys. Rev. D **67** (2003) 094007.
- 9 Cheng, H.-Y. and Chiang, C.-W., Phys. Rev. D **81** (2010) 074021.
- 10 Link, J. M. et al., Phys. Rev. D **75** (2007) 052003.
- 11 d'Argent, P. et al., JHEP **05** (2017) 143.
- 12 Baltrusaitis, R. M. et al., Phys. Rev. Lett. **56** (1986) 2140.
- 13 Li, H.-B. and Lyu, X.-R., Natl. Sci. Rev. **8** (2021) nwab181.
- 14 Ablikim, M. et al., Nucl. Instrum. Meth. A **614** (2010) 345.
- 15 Yu, C. et al., BEPCII Performance and Beam Dynamics Studies on Luminosity, in *7th International Particle Accelerator Conference*, page TUYA01, 2016.
- 16 Ablikim, M. et al., Chin. Phys. C **44** (2020) 040001.
- 17 Agostinelli, S. et al., Nucl. Instrum. Meth. A **506** (2003) 250.
- 18 Huang, K.-X. et al., Nucl. Sci. Tech. **33** (2022) 142.
- 19 Jadach, S., Ward, B. F. L., and Was, Z., Phys. Rev. D **63** (2001) 113009.
- 20 Jadach, S., Ward, B. F. L., and Was, Z., Comput. Phys. Commun. **130** (2000) 260.
- 21 Lange, D. J., Nucl. Instrum. Meth. A **462** (2001) 152.
- 22 Ping, R.-G., Chin. Phys. C **32** (2008) 599.
- 23 Workman, R. L. et al., PTEP **2022** (2022) 083C01.
- 24 Chen, J. C., Huang, G. S., Qi, X. R., Zhang, D. H., and Zhu, Y. S., Phys. Rev. D **62** (2000) 034003.
- 25 Yang, R.-L., Ping, R.-G., and Chen, H., Chin. Phys. Lett. **31** (2014) 061301.
- 26 Richter-Was, E., Phys. Lett. B **303** (1993) 163.
- 27 Ablikim, M. et al., Phys. Lett. B **734** (2014) 227.
- 28 Albrecht, H. et al., Phys. Lett. B **241** (1990) 278.
- 29 Amhis, Y. S. et al., Eur. Phys. J. C **81** (2021) 226.
- 30 Ablikim, M. et al., JHEP **05** (2021) 164.
- 31 Berger, N., Liu, B., and Wang, J., J. Phys. Conf. Ser. **219** (2010) 042031.
- 32 Von Hippel, F. and Quigg, C., Phys. Rev. D **5** (1972) 624.
- 33 Mandelstam, S., Paton, J. E., Peierls, R. F., and Sarker, A. Q., Annals Phys. **18** (1962) 198.
- 34 Herndon, D., Soding, P., and Cashmore, R. J., Phys. Rev. D **11** (1975) 3165.
- 35 Brehm, J. J., Annals Phys. **108** (1977) 454.
- 36 Rarita, W. and Schwinger, J., Phys. Rev. **60** (1941) 61.
- 37 Zemach, C., Phys. Rev. **140** (1965) B97.
- 38 Chung, S. U., Phys. Rev. D **57** (1998) 431.
- 39 Zou, B. S. and Bugg, D. V., Eur. Phys. J. A **16** (2003) 537.
- 40 Gounaris, G. J. and Sakurai, J. J., Phys. Rev. Lett. **21** (1968) 244.
- 41 Ablikim, M. et al., Phys. Lett. B **607** (2005) 243.
- 42 Anisovich, V. V. and Sarantsev, A. V., Eur. Phys. J. A **16** (2003) 229.
- 43 Aubert, B. et al., Phys. Rev. D **78** (2008) 034023.
- 44 Alexeev, G. D. et al., Phys. Rev. Lett. **127** (2021) 082501.
- 45 Aghasyan, M. et al., Phys. Rev. D **98** (2018) 092003.
- 46 Pivk, M. and Le Diberder, F. R., Nucl. Instrum. Meth. A **555** (2005) 356.
- 47 James, F. and Roos, M., Comput. Phys. Commun. **10** (1975) 343.
- 48 Efron, B., The Annals of Statistics **7** (1979) 1.
- 49 Langenbruch, C., Eur. Phys. J. C **82** (2022) 393.
- 50 Malde, S. et al., Phys. Lett. B **747** (2015) 9.
- 51 Ablikim, M. et al., Phys. Rev. D **106** (2022) 092004.
- 52 Ablikim, M. et al., Phys. Rev. D **106** (2022) 092005.
- 53 Ablikim, M. et al., Phys. Rev. D **97** (2018) 072004.
- 54 Bugg, D. V., J. Phys. G **34** (2007) 151.
- 55 Skwarnicki, T., *A study of the radiative CASCADE transitions between the Upsilon-Prime and Upsilon resonances*, PhD thesis, Cracow, INP, 1986.